

This discussion paper is/has been under review for the journal Atmospheric Measurement Techniques (AMT). Please refer to the corresponding final paper in AMT if available.

A novel instrument for measurements of BrO with LED based Cavity-Enhanced Differential Optical Absorption Spectroscopy

D. J. Hoch¹, J. Buxmann^{1,3,*}, H. Sihler^{1,2}, D. Pöhler¹, C. Zetzsch³, and U. Platt¹

¹Institute of Environmental Physics, University of Heidelberg, Heidelberg, Germany

²Max-Planck-Institute for Chemistry, Mainz, Germany

³Atmospheric Chemistry Research Laboratory, University of Bayreuth, Bayreuth, Germany

* now at: Met Office, Exeter, UK

Received: 16 May 2013 – Accepted: 28 May 2013 – Published: 2 July 2013

Correspondence to: U. Platt (ulrich.platt@iup.uni-heidelberg.de)

Published by Copernicus Publications on behalf of the European Geosciences Union.

Title Page

Abstract

Introduction

Conclusions

References

Tables

Figures

◀

▶

◀

▶

Back

Close

Full Screen / Esc

Printer-friendly Version

Interactive Discussion



Abstract

The chemistry of the troposphere and specifically the global tropospheric ozone budget is affected by reactive halogen species like Bromine monoxide (BrO) or Chlorine monoxide (ClO). Especially BrO plays an important role in the processes of ozone destruction, disturbance of NO_x and HO_x chemistry, oxidation of DMS, and the deposition of elementary mercury. In the troposphere BrO has been detected in polar regions, at salt lakes, in volcanic plumes, and in the marine boundary layer. For a better understanding of these processes field measurements as well as reaction-chamber studies are performed. In both cases instruments with high spatial resolution and high sensitivity are necessary. A Cavity Enhanced Differential Optical Absorption Spectroscopy (CE-DOAS) instrument with an open path measurement cell was designed and applied. For the first time, a CE-DOAS instrument is presented using an UV-LED in the 325–365 nm wavelength range. In laboratory studies, BrO as well as HONO, HCHO, O₃, and O₄, could be reliably determined at detection limits of 20 ppt for BrO, 9.1 ppb for HCHO, 970 ppt for HONO, and 91 ppb for O₃, for five minutes integration time, respectively. The best detection limits were achieved for BrO (11 ppt), HCHO (5.1 ppb), HONO (490 ppt), and O₃ (59 ppb) for integration times of 81 min or less. Comparison with established White-System DOAS and O₃ monitor demonstrate the reliability of the instrument.

1 Introduction

Besides their well known effects on stratospheric ozone, Reactive Halogen Species (RHS) are responsible for a series of phenomena in various compartments of the troposphere including volcanic plumes, coastal areas, salt lakes, and the polar boundary layer. For instance, RHS, and especially bromine, are of scientific interest, because they are mainly responsible for ozone depletion in the arctic boundary layer during polar spring. The phenomenon was first observed by Bottenheim et al. (1986), and sev-

AMTD

6, 6047–6096, 2013

BrO CE-DOAS

D. J. Hoch et al.

Title Page

Abstract

Introduction

Conclusions

References

Tables

Figures

⏪

⏩

◀

▶

Back

Close

Full Screen / Esc

Printer-friendly Version

Interactive Discussion



[Title Page](#)[Abstract](#)[Introduction](#)[Conclusions](#)[References](#)[Tables](#)[Figures](#)[◀](#)[▶](#)[◀](#)[▶](#)[Back](#)[Close](#)[Full Screen / Esc](#)[Printer-friendly Version](#)[Interactive Discussion](#)

eral other studies followed, which established a link between O₃-depletion and RHS (e.g. Barrie et al., 1988, 1994; Hausmann M. and Platt U., 1994; Bottenheim et al., 1990; Sturges et al., 1993; Platt and Lehrer, 1996; Kreher et al., 1997; Tuckermann et al., 1997). The halogen catalyzed ozone depletion events occur only during polar sunrise. The release mechanism for reactive bromine is described by the “bromine explosion” mechanism (Platt and Lehrer, 1996). The phenomenon is still not completely understood and is subject of current research (Saiz-Lopez et al., 2007; Pöhler et al., 2010; Friess et al., 2011).

Also outside polar regions RHS strongly affect the ozone budget and the oxidation capacity of the atmosphere. BrO was detected in the mid-latitude marine boundary layer at different locations (Leser et al., 2003; Saiz-Lopez et al., 2004; Read et al., 2008; Mahajan et al., 2010). At salt lakes high mixing ratios of BrO could be detected, up to 20 ppt at the Salar de Uyuni, Bolivia (Hönninger et al., 2004) and up to 220 ppt at the Dead Sea (Hebestreit et al., 1999; Matveev et al., 2001; Tas et al., 2008). Most of these observations were performed with LP-DOAS or MAX-DOAS measurement techniques averaging the concentration over several kilometers. For a better understanding of the involved processes, field measurements with high spatial resolution are essential. CE-DOAS offers the opportunity of mobile in-situ measurements of RHS, without the risk of inlet and wall losses. In addition, RHS release, transformation, and loss processes can be studied in reaction chambers (e.g. Buxmann et al., 2012; Ofner et al., 2012). For these studies also compact yet highly sensitive instruments for RHS measurements are required.

O’Keefe and Deacon (1988) started to use optical cavities with high reflective mirrors to observe absorbers by applying Cavity-Ringdown (CRD) spectroscopy. With this approach, the decay of light intensity leaking from the resonator after switching off the pump light source is measured. Since then the technique was continuously refined (Zalicki and Zare, 1995; Paldus et al., 2000; Ball et al., 2001; Fawcett et al., 2002; Simpson, 2003; Ball and Jones, 2003; Schuster et al., 2009). A shortcoming of most CRD instruments is that any absorptions beside that of the investigated trace gas for the used

BrO CE-DOAS

D. J. Hoch et al.

Title Page

Abstract

Introduction

Conclusions

References

Tables

Figures

◀

▶

◀

▶

Back

Close

Full Screen / Esc

Printer-friendly Version

Interactive Discussion



wavelength lead to false signals and must be avoided. This requires typically closed resonators with aerosol inlet filters and thus introducing the risk of losses on the inlet and filter, as well as possible chemical reactions. A second approach, the so-called Cavity Enhanced Absorption Spectroscopy (CEAS), was developed, which relies on measuring the transmittance of the resonator by recording the leak-out intensity (Engeln et al., 1998; Peeters et al., 2000). In contrast to CRDS the CEAS approach uses a continuous wave (CW) source of radiation. Based on CEAS (e.g. Fiedler et al., 2003; Langridge et al., 2006; Venables et al., 2006; Orphal and Ruth, 2008; Vaughan et al., 2008; Washenfelder et al., 2008; Langridge et al., 2008; Varma et al., 2009; Chen and Venables, 2011; Chen et al., 2011; Kahan et al., 2012 applied the Broad Band (BB) CEAS using broad band light sources (rather than a single wavelength as in the traditional CRDS or CEAS approaches). Ball et al. (2004) combined BBCEAS for the data evaluation with the established DOAS technique (Platt and Stutz, 2008), creating the CE-DOAS. With this technique different trace gases could be detected simultaneously and at high spatial resolution (Ball et al., 2004; Gherman et al., 2008; Platt et al., 2009; Meinen et al., 2010; Thalman and Volkamer, 2010). We note that the BBCEAS retrieval algorithm published by Fiedler et al. (2003) relies – like DOAS – on the characteristic narrow band absorption features of the molecules for their quantification and is thus in principle equivalent to DOAS. The theoretical description of CE-DOAS can be found in Platt et al. (2009). Up to date, to our knowledge, only two cavity based measurement systems to detect BrO in the UV-wavelength range exist (Chen and Venables, 2011; Grilli et al., 2012), but none applies the DOAS technique. Both of them use a heavy and highly power consuming light source (e.g. tunable laser and Xenon-arc lamp). This means that there is a lack of in-situ instruments allowing direct measurement of the BrO radicals, especially for field application.

Besides cavity instruments, Chemical Ionization Mass Spectrometers (CIMS) are capable of indirect BrO detection, but complex sample preparation and calibration is needed (e.g. Neuman et al., 2010; Liao et al., 2011). This limits the application of these instruments for field studies where low power and a lightweight setup is required.

BrO CE-DOAS

D. J. Hoch et al.

Title Page

Abstract

Introduction

Conclusions

References

Tables

Figures

◀

▶

◀

▶

Back

Close

Full Screen / Esc

Printer-friendly Version

Interactive Discussion



Furthermore the transportable mode-locked frequency-doubled cavity-enhanced spectrometer described by Grilli et al. (2012) has a 7 m Teflon inlet system. Although the instrument provides BrO detection with remarkable good detection limits of 1.7 ppt at a time resolution of 30 s, the effect of inlet loss was not investigated so far. The authors state undetectable BrO losses within the relatively large concentration fluctuations of up to ± 12 ppt. This result does need further confirmation, since from indirect detection of BrO with CIMS instruments, it is well known, that loss or chemical conversion of highly reactive compounds (e.g. BrO or HOBr), on instrument and inlet surfaces occur and can even result in a complete loss of BrO (Neuman et al., 2010). Such a characterisation is still missing for CE-spectrometers as described by Grilli et al. (2012). It was demonstrated by Liao et al. (2011) that reliable BrO concentrations can be provided by an optimised and very short inlet CIMS instrument, and that losses on inlets can be largely avoided or corrected. These measurements were found to be in good agreement with a well established long-path DOAS system (Liao et al., 2011).

Our paper describes the design and development of a specific CE-DOAS instrument, which, for the first time, identifies BrO in the UV-wavelength range (325–365 nm) by applying an UV-LED. Compared to the xenon arc lamp applied as light sources in previous experiments, UV-LEDs offer several advantages particularly important for cavity enhanced measurements: (1) the relatively narrow emission spectrum of LEDs reduces the amount of straylight within the instrument, because there is no light emitted outside the spectral range of the high mirror reflectivity. Hence, fewer spectral filters are required, the risk of systematic measurement errors is reduced and the instrument setup becomes less complex. (2) The light output of LEDs may be easily modulated. It is thus possible with the instrument presented here, to monitor the effective path length by measuring the ring-down time between measurements. (3) The lifetime of LEDs is typically longer than for arc lamps. This reduces the maintenance and the costs of operation are lowered. (4) LEDs are much easier to handle than arc lamps and do not e.g. require a special housing or high voltage for ignition. The power consumption is by far lower, as mentioned above, and less excess heat is produced. This is partic-

ularly useful when the light-source is applied in temperature controlled environments like smog chambers.

Compared to instruments designed for the VIS/IR wavelength range, Rayleigh scattering and parasitic mirror losses become important in the UV and thus reduce the achievable maximum path length. Both effects are discussed in this paper. To estimate the optical path length in the cavity, the instrument applies CRD-technique (Meinen et al., 2010) and additionally the measurements of the trace gases O_4 , O_3 , and HONO. At the Atmospheric Chemistry Research Laboratory of the University of Bayreuth, Germany, first laboratory measurements were successfully performed and the detection limits for different trace gases were determined. Also, we present an intercomparison with an established White-System DOAS and a CL monitor for ozone detection.

2 Method: Cavity-Enhanced Differential Absorption Spectroscopy (CE-DOAS)

The basic idea of the CE-DOAS technique is to introduce incoherent broadband radiation with the intensity I_L into an optical resonator (see Fig. 1), consisting of two mirrors with reflectivity R (for simplicity we assume both mirrors to have the same reflectivity, if the mirrors have different reflectivities R_1 , R_2 an averaged reflectivity $R = \sqrt{R_1 R_2}$ is used). The distance between the mirrors is d_0 (see Fig. 1). Initially only the fraction $\rho = 1 - R$ of the radiation I_L enters the resonator. Here for simplicity I_L means only the fraction of the radiation from the LED which can be imaged into the resonator. (It is obvious that not all radiation emitted by the LED is passing through the lens and also passes the aperture defined by mirror M_2 .) Once inside the resonator, the radiation is reflected on average $1/(1 - R)$ times (neglecting other losses). Finally, in the absence of any extinction in the resonator, half of the radiation leaves the resonator through each mirror. The radiation (intensity I_{tot}) leaving the cavity through the mirror opposite to the light source (see Fig. 1) is available for further analysis as described below.

The DOAS techniques derive the trace gas concentration by the use of the optical density $D(\lambda)$ which requires the measurement of the intensities without ($I_0(\lambda)$) and

Title Page

Abstract

Introduction

Conclusions

References

Tables

Figures

◀

▶

◀

▶

Back

Close

Full Screen / Esc

Printer-friendly Version

Interactive Discussion



with $I(\lambda)$ trace gas absorption (Platt and Stutz, 2008). In a CE-DOAS setup the optical density $D_{CE(\lambda)}$ is determined from intensity measurements with absorber free filled (e.g. synthetic air) resonator I_{tot0} and with sample air filled resonator I_{tot} (Platt et al., 2009):

$$D_{CE(\lambda)} = \ln \left(\frac{I_{tot0}(\lambda)}{I_{tot}(\lambda)} \right) = \ln \left(\frac{\int_0^{\infty} I_{in0}(\lambda, n) dn}{\int_0^{\infty} I_{in}(\lambda, n) dn} \right). \quad (1)$$

$I_{in0}(n)$ is the intensity after n passes through the cavity in the pure air filled cavity (without any absorbers) and $I_{in}(n)$ is the intensity after n passes through the cavity including also absorptions. n is the number of traverses of the photons through the cavity. However according to Platt et al. (2009) for strong absorptions this is not equal to the optical density $D(\lambda)$ used in traditional DOAS application if using the average light path from Sect. 2.1. Thus, the corrections described in Sect. 2.3 have to be applied.

2.1 Determination of the average path length

A theoretical description of the average path length can be found in Platt et al. (2009). In practice, this average path length $\bar{L}_0(\lambda)$ can be determined from the known Rayleigh scattering of two different gases, e.g. Helium and dry zero air (Washenfelder et al., 2008), from a CRD decay time measurement (Meinen et al., 2010), or from the differential absorption of a trace gas of known concentration. In this work $\bar{L}_0(\lambda)$ was determined from the absorption bands of O_4 at 343.5 and 360.4 nm making use of the known O_2 concentration (Ball et al., 2004). The following subsections describe, how this average path length has to be corrected.

Title Page

Abstract

Introduction

Conclusions

References

Tables

Figures

⏪

⏩

◀

▶

Back

Close

Full Screen / Esc

Printer-friendly Version

Interactive Discussion



2.2 Correction of the base path-length

The length of the absorption medium in the resonator d is not necessarily equal to the distance between the mirrors d_0 (see Fig. 2), since at either end of the resonator usually a few centimeters of the path are not filled with sample air due to a purge flow close to the mirrors. In this case, the effective light path has to be corrected by the geometric factor d/d_0 .

$$\bar{L}(\lambda) = \bar{L}_0(\lambda) \frac{d}{d_0} \quad (2)$$

For measurements of a small sample volume (small chamber), the dilution of the air due to the purge flow has also be taken into account.

2.3 Correction for light path reduction due to extinction in the cavity

Platt et al. (2009) describe in detail how the light path is reduced by extinction in the resonator. Here two ways to correct this effect presented by Platt et al. (2009) are applied. A more detailed explanation of method 1 can be found in Horbanski (2010); Horbanski et al. (2012). For both ways the optical density D_{CE} and the average path length $\bar{L}(\lambda)$ needs to be known.

1. Correction of the trace gas absorption cross section σ to σ_{eff} :

$$\sigma_{\text{eff}}(\lambda) = \sigma(\lambda) \times \frac{\bar{L}_{\text{eff}}(\lambda)}{\bar{L}(\lambda)} = \sigma(\lambda) \times \frac{D_{CE}}{e^{D_{CE}} - 1}. \quad (3)$$

This σ_{eff} is used by a DOAS-fit to obtain a corrected column density. From this column density the correct concentration is determined by dividing with $\bar{L}(\lambda)$. As the absolute optical density D_{CE} is difficult to measure precisely, this method is used iteratively, where the optical density D_i of the i -th iteration is calculated.

Title Page

Abstract

Introduction

Conclusions

References

Tables

Figures

⏪

⏩

◀

▶

Back

Close

Full Screen / Esc

Printer-friendly Version

Interactive Discussion



During the first iteration a DOAS fit determines an optical density D_0 and σ_0 is corrected to σ_1 . In the next iteration step σ_1 determines a D_1 and σ_0 is corrected to σ_2 , etc:

i. iteration:

$$\sigma_i \rightarrow (\text{cL})_i \rightarrow (\text{cL})_i \times \sigma_i = D_i \rightarrow \sigma_0 \times \frac{D_i}{e^{D_i} - 1} = \sigma_{i+1}. \quad (4)$$

We applied this correction in four iteration steps, for measurements with only one trace gas and without aerosols. The same method can also be applied if several absorbers are present by extending Eq. (4). This method has the large advantage that it does not rely on the absolute optical density D_{CE} and thus intensity I_{tot} and is thus not sensitive to any possible intensity changes of e.g. the LED between reference and sample measurement.

2. Method 1 with Eq. (3) becomes very complex when using more than one absorber and is not applicable if aerosols are present. In this case, a second method is useful in order to correct the optical density before the fit and convert it to D_{eff} which is equal to an absorption where the light path is not reduced:

$$D_{\text{eff}} = e^{D_{\text{CE}}} - 1 = \frac{I_{0\text{tot}}}{I_{\text{tot}}} - 1. \quad (5)$$

In this work, the second method applying Eq. (5) is used whenever there is more than one absorber. It needs to be considered that for this correction the intensities $I_{0\text{tot}}$ and I_{tot} have to be successively measured. This requires an absolutely stable optical resonator and light source intensity, similar to the requirements of the BBCEAS approach.

Title Page

Abstract

Introduction

Conclusions

References

Tables

Figures

⏪

⏩

◀

▶

Back

Close

Full Screen / Esc

Printer-friendly Version

Interactive Discussion



2.4 Correction of the wavelength dependence of the average light path

As described in Sect. 2.1, the average light path $\bar{L}(\lambda)$ is dependent on λ also because $R(\lambda)$ is dependent on λ . As described by Venables et al. (2006) it is possible to use differential absorption structures for the determination of the wavelength dependence of the mirror reflectivity and therefore for the calibration of the path length. This method requires an absorber of known concentration, which has several distinct absorption bands in the wavelength range of interest. However, the relative shape of the mirror reflectivity curve can be determined from any absorber having several absorption bands within the region of high mirror reflectivity. In the present study, we used O_3 and HONO to estimate the shape of the reflectivity curve. Since the concentration of these gases was unknown the absorption bands of O_4 at 343.5 and 360.4 nm were additionally used to derive the absolute reflectivity curve of the mirrors.

3 Experimental

3.1 Instrument

Figure 1 shows a schematic diagram of the CE-DOAS instrument (more details can be found at Hoch, 2010). The radiation of a pulsed UV-LED is imaged by lens L_1 into the resonator, consisting of two high reflective dielectric mirrors M_1 and M_2 (focal length = 1 m). The radiation, which leaves the resonator through M_2 , is focused by the lens L_2 into a fiber bundle which can be adjusted by a x - y translation stage. This fiber bundle transmits the light to a temperature-stabilized spectrograph (see section). The movable mirror “ K ” can redirect the light to a photomultiplier (PMT) to record a ring-down signal and thus check the quality of the resonator. F_1 and F_2 are band-pass filters (for details see Sect.). F_1 protects the PMT and F_2 shields the fibers from scattered light and LED light outside of the reflectivity range of the mirrors. The shutter is used to perform background measurements without radiation of the UV-LED. The electronic

Title Page

Abstract

Introduction

Conclusions

References

Tables

Figures

◀

▶

◀

▶

Back

Close

Full Screen / Esc

Printer-friendly Version

Interactive Discussion



controller receives a constant current and creates the pulses for the UV-LED. It also controls the shutter and the mirror “K”.

3.1.1 LED radiation source

The wavelength range (325 to 365 nm) of the LED UVTOP340 from Sensor Electronic Technology was chosen to optimize the sensitivity to BrO while minimizing the interference due to O₃, but still being appropriate to detect O₃. In the order to minimize the known LED etalon structures the surface-normal of the LED-chip is inclined against the optical axis of the resonator at an angle of 15° (Sihler et al., 2009). For CRD-measurements the LED has to be operated in a pulsed mode. Extensive noise characterizations of the LED showed that permanent pulsing of the LED creates less spectral noise than a periodic change between pulsing and continuous operation, while the spectrum of the LED does not change. Therefore the LED is permanently pulsed with 750 μs (on) and 50 μs (off) also for recording spectra with the spectrometer. The time for the cavity to reach optical equilibrium is approximately 3.7 μs (for mirrors of reflectivity 0.9991) and 1 m cavity length) leading to a maximum light path of approximately 1111 m. This is small relative to the 750 μs when the LED is powered.

The UVTOP340 delivers 400 μW of optical output power (SET, 2010). This figure appears incredibly small now compared to the optical output power of a 75 W xenon arc lamp as described by Kern et al. (2006). However, the relevant quantity needed to compare the optical output of different light sources is the spectral radiance integrated over the wavelength interval used to evaluate for the trace gas absorption features. On the one hand, the radiance of the UVTOP340 between 325 and 365 nm calculates to $4.2 \times 10^3 \text{ Wm}^{-2} \text{ sr}^{-1}$ assuming a Lambertian emission pattern, an emitter area of 0.045 mm² as derived from microscopic measurements, and a Gaussian emission spectrum (340 nm peak, 15 nm FWHM). On the other hand, the emission spectrum of a xenon arc lamp (e.g. XBO 75W/2 xenon arc lamp manufactured by OSRAM) is approximated by that of a Planckian gray-body with an emissivity of 0.17 derived from the photometric properties given in Osram (2012). The radiance of the xenon arc lamp

Title Page

Abstract

Introduction

Conclusions

References

Tables

Figures

⏪

⏩

◀

▶

Back

Close

Full Screen / Esc

Printer-friendly Version

Interactive Discussion



Title Page

Abstract

Introduction

Conclusions

References

Tables

Figures

◀

▶

◀

▶

Back

Close

Full Screen / Esc

Printer-friendly Version

Interactive Discussion



between 325 and 365 nm calculates to $1.9 \times 10^6 \text{ Wm}^{-2} \text{ sr}^{-1}$. Thus, the arc lamp has a radiance in this wavelength interval which is about 450 times higher compared to the UVTOP340. However, the optical output power in the 325 to 365 nm range per electrical input power for both devices is almost equal since the UVTOP340 consumes only 180 mW.

3.1.2 Mirrors and optics

The main component of the setup is the resonator which consists of two highly reflective mirrors (Fig. 1, M_1 and M_2). The reflectivity of the mirrors from LAYERTEC GmbH, (Mellingen, Germany) was chosen to achieve a good compromise between optical light path length and signal to noise ratio (Fiedler et al., 2007). The radiation of the UV-LED is coupled into the resonator by lens L_1 ($F_1 = 25 \text{ mm}$) to use as much of the LED output as possible. The radiation which passes mirror M_2 is focused by lens L_2 ($F_2 = 100 \text{ mm}$) on a fiber coupler to match the numerical aperture (NA^1) of the spectrometer. The fiber bundle (Loptek GmbH & Co, Berlin, Germany) consists of seven 200 μm fibers (NA of 0.22, UV solarization stabilized, 6 m long), arranged in a circular configuration on the resonators side and column configuration at the spectrometers side. The band-pass filter F_1 and F_2 , both UG11 from Schott, (Mainz, Germany) have a transmission range of 270–380 nm and a thickness of 1 mm. F_1 was placed directly in front of the PMT protect the device as much as possible against ambient light (e.g. if cover is opened). The reflectivity of the mirrors can not readily be derived from the manufacturer's data: Layertec provided transmission values (T) but not reflectivities. Since $R + T + A = 1$ ($A = \text{Absorption}$) R can not be calculated from T unless the absorption A in the dielectric mirror is negligible, which, unfortunately, is not the case in this wavelength range. We used two sets of mirrors with different values of stated transmissivity at 340 nm: M_1 : $T = 0.048 \%$, M_2 : $T = 0.11 \%$.

¹ $\text{NA} = n \sin(\alpha/2)$, $n = \text{index of refraction} = 1.0$ (air), $\alpha = \text{angular aperture}$ (maximum cone of light that can enter or exit the optical device of interest).

3.1.3 Spectrograph and detector

The fiber transmits the light into a temperature stabilized ((20.0 ° ± 0.1) C) spectrograph QE65000 from Ocean Optics (Dunedin, Florida, USA). The spectrometer has a focal length of 101 mm, it is equipped with a 2400 lines mm⁻¹ grating resulting in 0.62 nm spectral resolution with the column of seven 200 μm fibers (see Sect. 3.1.2) acting as entrance slit.

The detector used in the QE65000 spectrometer is a scientific-grade, back-thinned, Thermo-Electrically Cooled (TEC), 1044 × 64 element CCD array (S7031-1006 from Hamamatsu Photonics (Naka-ku, Hamamatsu City, Shizuoka Pref., Japan)), temperature stabilized to -20°C.

3.1.4 Photomultiplier (PMT) for CRD

For the ring down measurement the radiation intensity is measured by a PMT (H578-01 from Hamamatsu Photonics (Naka-ku, Hamamatsu City, Shizuoka Pref., Japan)). As current amplifier a DLPCA-100 from FEMTO Messtechnik GmbH, (Berlin, Germany) is applied. A PC-oscilloscope DAQSCOPE PCI-5102 from National Instruments (Austin, Texas, USA) records the ring down signal.

3.1.5 Software

The program DOASIS (Kraus, 2004) is used to control the measurements and to analyze the CE-DOAS and White-System DOAS spectra.

To acquire the CRD signals a dedicated program was developed with LabVIEW from National Instruments. This program receive the ring down signal from the PC-oscilloscope, calculates the mean of a given number of measurements and fits a double exponential decay $f(t)$ (Eq. 6).

$$f(t) = A \times \left(\frac{\tau_1}{\tau_1 - \tau_2} \times e^{-\frac{t}{\tau_1}} - \frac{\tau_2}{\tau_1 - \tau_2} \times e^{-\frac{t}{\tau_2}} \right) + b \quad (6)$$

Title Page

Abstract

Introduction

Conclusions

References

Tables

Figures

◀

▶

◀

▶

Back

Close

Full Screen / Esc

Printer-friendly Version

Interactive Discussion



[Title Page](#)[Abstract](#)[Introduction](#)[Conclusions](#)[References](#)[Tables](#)[Figures](#)[Back](#)[Close](#)[Full Screen / Esc](#)[Printer-friendly Version](#)[Interactive Discussion](#)

τ_1 denotes the electro-optical decay time from electronics and LED and τ_2 for the CRD-decay time. Also A denotes the initial signal at $t = 0$ and b denotes any offset signal at $t = \infty$. From this fit and known τ_1 the CRD-decay time can be determined and converted to a optical light path or mirrors reflectivity according to Meinen et al. (2010).

5 However in our case it is not possible to derive with this method the accurate absorption light path for the data evaluation, as the mirror reflectivity varies too much over the LED spectral range (see Sect. 2.4). Nevertheless, τ_2 just gives an indication of the wavelength averaged light path, which is used to monitor the contamination of the mirrors as well as the optical alignment of the resonator. This allows quick action to
10 the optimize instrument performance. In fact during chamber studies the UV-CE DOAS system performed with excellent stability during a time period of several days without mirror cleaning and readjustment.

3.2 The measurement setups

The instrument was developed and characterized at the Institute for Environmental
15 Physics (IUP) in Heidelberg, Germany. After first successful measurements, it was applied for the observation of different trace gases at the Atmospheric Chemistry Research Laboratory, University of Bayreuth, Germany. For these measurements the instrument was used as it is described in Sect. 3.1 and shown in Fig. 1. Two hermetically sealed plastic boxes were placed around the optical component assemblies in order
20 to protect the sensitive optics against dust and other extreme conditions for planned measurements in a climate chamber. Furthermore the hermetically sealed containment guarantees a stable nitrogen purge-flow (1 L min^{-1}) of the resonator mirrors to prevent contaminations from the measurement air. Otherwise a slight overpressure in the reaction chamber could cause a flow of unfiltered air from the chamber towards
25 the mirrors and thus cause contaminations. For the measurements described in the following an air tight chamber was placed between the two boxes containing the mirrors and associated optics (Fig. 2). This chamber could be filled through three gas inlets/outlets with different gases. Three different set-ups with various base-path lengths

[Title Page](#)[Abstract](#)[Introduction](#)[Conclusions](#)[References](#)[Tables](#)[Figures](#)[◀](#)[▶](#)[◀](#)[▶](#)[Back](#)[Close](#)[Full Screen / Esc](#)[Printer-friendly Version](#)[Interactive Discussion](#)

were used: one with a glass chamber (setup A) and two with Teflon chambers (setup B and C). The glass chamber set up was the first to be used, because it could be built easier than Teflon, but the cavity length is much shorter. In order to determine the path length it is useful to have different cavity lengths. The Teflon/glas chambers A, B and C were kept in pressure equilibrium with the laboratory, with the help of two open outlets as indicated in Fig. 2. The mirror purge flow compensates for any leakage of the chamber. Table 1 shows the sizes of these three chambers and Table 2 gives an overview of the different trace gas measurement setups. With these setups, different trace gas measurements were carried out: O₃ and HONO were measured mainly in order to determine the wavelength dependency of the mirror reflectivity and the optical path length, O₄ measurements were performed in order to determine the absolute optical path length at two particular wavelengths (343.4 and 360.5 nm) and BrO and HCHO measurements were made in order to determine the detection limits for these species. Before each trace gas measurement, offset (20 000 scans and 8 ms integration time) and dark current (1 scan and 30 000 ms integration time) spectra were taken with blocked LED. If any background radiation intensity would be present, it would be included in the dark current spectrum. In the next step a CRD measurement with 1000 average determinations was performed to determine possible mirror contamination. A spectrum with 85 % of full saturation could be obtained in 9.50 s with mirror set M_1 and 3.50 s with mirror set M_2 . Based on noise tests, 30 spectral scans were taken and co-added for mirror set M_1 and 50 spectral scans were taken and co-added for mirror set M_2 to achieve sufficient measurement accuracy. This corresponds to a temporal resolution of 4.8 min for M_1 and 2.9 min for M_2 . The measurements shown within this study were undertaken without the presence of aerosols.

3.2.1 Ozone measurements

For the O₃ measurements the setups A, B, and C were used. For setup A both mirror sets, for setup B mirror set M_2 , and for setup C mirror set M_1 were used (Table 2). To determine an I_0 spectrum the chamber was filled with nitrogen and the

[Title Page](#)[Abstract](#)[Introduction](#)[Conclusions](#)[References](#)[Tables](#)[Figures](#)[⏪](#)[⏩](#)[◀](#)[▶](#)[Back](#)[Close](#)[Full Screen / Esc](#)[Printer-friendly Version](#)[Interactive Discussion](#)

mirrors were purged with nitrogen, too. Afterwards O_3 was produced and filled into the chamber through the gas inlet (up to 2 ppm). The gas outlets were connected to an active charcoal trap. In setup A and B the ozone was created by ionization of O_2 (purity = 99.995 %) using a corona discharge ozonizer and in setup C by passing O_2 (purity = 99.995 %) along four pen-ray mercury discharge lamps.

3.2.2 Nitrous acid measurements

For the nitrous acid (HONO) measurements setup A with both mirror sets, setup B with mirror set M_2 , and setup C with mirror set M_1 were used (see Table 2), similar to the setup for O_3 measurements. The generation of the nitrous acid is based on the reaction of a sodium nitrite solution $NaNO_2$ with sulfuric acid H_2SO_4 as e.g. described by Taira and Kanda (1990):



The reaction takes place in a glass vessel with a glass frit at its base. The diluted solutions of sodium nitrite and sulfuric acid are continuously pumped into a reaction vessel and the mixture is then drawn off to waste. A carrier gas, here nitrogen, is introduced into the reagent mixture through the frit and continuously purges nitrous acid vapor from the mixture. The HONO generation depends on temperature, gas flow, $NaNO_2$ concentration and fluid flow. Typical mixing ratios up to 30 ppb were accomplished.

3.2.3 Oxygen dimer measurements

In order to determine the light path in the cavity O_4 measurements were carried out, at two particular wavelengths (343.4 and 360.5 nm). For that purpose the resonator was first completely filled with nitrogen and afterwards completely (including mirror purge gas) with pure oxygen. Additionally barometric pressure (with a mercury barometer) and temperature were measured next to the chamber (the same values assumed as in

the chamber) to determine the O₂ concentration in the resonator. With the absorption of O₄ at 343.4 and 360.5 nm the light path at these wavelengths could be determined.

3.2.4 Bromine monoxide measurements

BrO measurements were carried out using setup B with mirror set M_2 and in setup C with mirror set M_1 (see Table 2). For these measurements the mirror protection tubes were purged with nitrogen. The gas outlets are connected to a pump producing a slight underpressure. First O₃ was admitted through the gas inlet and afterwards Br₂. A fluorescent tube (Philips TL/12, 40W, UV A and UV B) set up next (at 20 cm distance) to the chamber was switched on to photolyze Br₂. A typical concentration up to 1000 ppt BrO was measured. Evaluation and results of these measurements are described in Sect. 4.

3.2.5 Comparison of the CE-DOAS with a White-System DOAS and an ozone monitor

During experiments with a simulated salt pan (Buxmann et al., 2012) at the Atmospheric Chemistry Research Laboratory, University of Bayreuth, Germany, in the low-temperature aerosol simulation chamber (LOTASC) (<http://www.eurochamp.org/chambers/lotasc/>) a comparison between the CE-DOAS and a White-System (WS) (White, 1942, 1976; Ritz et al., 1993; Volkamer, 1996; Volkamer et al., 2002; Hak et al., 2005) as well as the CE-DOAS and an chemiluminescence-ozone monitor (CL, Bendix-UPK8002) was performed. The cylindrical chamber, made of Teflon foil (FEP 200 A, DuPont, thickness 0.05 mm) with a diameter of 1.33 m and a volume of 3500 L has been described in detail by Siekmann (2008); Bleicher (2012); Buxmann et al. (2012). The LOTASC was kept at a pressure slightly above atmospheric pressure in order to prevent leaking of room air into the system. The dilution rate, replenishing the loss by sampling and other outlets, was of the order of $3 \times 10^{-5} \text{ s}^{-1}$, which corresponds to about 4 L min^{-1} zero air input, including the purge flow (1 L min^{-1}) of the CE-DOAS

Title Page

Abstract

Introduction

Conclusions

References

Tables

Figures

⏪

⏩

◀

▶

Back

Close

Full Screen / Esc

Printer-friendly Version

Interactive Discussion



[Title Page](#)[Abstract](#)[Introduction](#)[Conclusions](#)[References](#)[Tables](#)[Figures](#)[◀](#)[▶](#)[◀](#)[▶](#)[Back](#)[Close](#)[Full Screen / Esc](#)[Printer-friendly Version](#)[Interactive Discussion](#)

mirrors (compare Buxmann et al., 2012 and Buxmann, 2012). The dilution rate is monitored using n-perfluorohexane as inert dilution standard. Several ppb of the standard are added before starting the experiment and measured by a gas chromatograph with flame ionization detector (GC-FID, Sichromat; Siemens, Karlsruhe, Germany) with a capillary column (Al_2O_3) porous layer open tubing (PLOT); Chrompack, Middelburg, the Netherlands) to provide the radical clock method, as described by Buxmann et al. (2012), Bleicher (2012) and references therein.

During the intercomparison experiments the WS had a base path of 2 m and an aperture of F/25, with a total light path of 288 m diagonally arranged through the chamber, whereas the CE-DOAS light path was horizontally arranged with a mirror distance of 1.33 m. In order to determine the absolute light path in the cavity, O_4 measurements were carried out, as described above. For that purpose an additional tube was mounted in between the resonator inside the smog chamber. The maximal path length at 346.3 nm was 816 m. A sketch of the experiment set up is shown in Fig. 9. These experiments were described in detail by Buxmann (2012) and the results are described in Sect. 4.3.

4 Data evaluation and results

The software DOASIS (Kraus, 2004) was used for the analysis of the recorded spectra as described in Sect. 3.1. The wavelength calibration of the spectrometer/detector was done with the help of the line spectra of a mercury lamp. For convolution of the literature absorption cross sections (overview in Table 3) with the instrument function the recorded line shape at 334.14 nm of this lamp was used. For each trace gas a mean-spectral shift was determined from a measured spectrum with strong absorption and the cross sections were corrected with these mean shift (Pre-shift, see Table 3) and linked together during the fit-routine. For all trace gases the following DOAS-fit settings were used: fit window 325–365 nm; high pass filter with 1000 iterations; 3rd degree polynomial; spectral squeeze/stretch limited to $\pm 2\%$ (of the total spectral range).

4.1 Mirror reflectivity and path length calibration

As described in Sect. 2.4 it is possible to use differential absorption structures to derive the wavelength dependence of the mirror reflectivity and therefore for the determination of the wavelength dependent path length.

We used O_3 and HONO to estimate the relative shape of the mirror reflectivity, not the absolute, as the actual concentrations of O_3 and HONO were unknown. The used fit windows are shown in Table 4. The relative shape was derived using a second-order polynomial fit, and the sensitivity of the O_3 and HONO measurements result in a maximal uncertainty of the relative shape of the reflectivity within the fitting range of 0.05 %. With the additional absorption bands of O_4 at 343.4 and 360.5 nm, the absolute reflectivity curve of the mirrors could be determined with known concentration of O_4 . The absolute reflectivity curves are shown in Fig. 3. The accuracy of the absolute reflectivity curves depends on the sensitivity of the HONO, O_3 and O_4 measurements. It is dominated by the sensitivity of the O_4 measurements, which is estimated according to Stutz and Platt (1996) to 2%. Thus the total error of the absolute path length is estimated at 2%. The following measurements were corrected with those reflectivity curves. The absorption A of the mirrors can be derived from the data in Fig. 3 as:

$$A = (1 - T) - R. \quad (7)$$

The absorptions of both mirror sets are of the order of $A = 4 \times 10^{-4}$. According to Fiedler et al. (2007) the relation between optical light path length and signal to noise ratio Q can be determined with:

$$Q = \frac{(1 - R - A) \left[1 + (1 - L)^2 R^2 \right]}{\sqrt{\left[1 - (1 - L)^2 R^2 \right]^3}}. \quad (8)$$

Figure 4 shows the enhancement factor (quality factor) Q dependency on $(1 - R)$ assuming $A = 4 \times 10^{-4}$. Based on this theory, we expected a lower detection limit for a

Title Page

Abstract

Introduction

Conclusions

References

Tables

Figures

⏪

⏩

◀

▶

Back

Close

Full Screen / Esc

Printer-friendly Version

Interactive Discussion



reflectivity of $R_2 = 0.9984$ of M_2 than for M_1 ($R_1 = 0.9991$), if the measurement accuracy is purely dominated by photon noise.

4.2 Detection limits

The true 1σ error of the measurement for the different trace gases are obtained from the statistical 1σ error of the DOAS fit, by multiplying with a factor of of about 2.5 (depending on the ratio between width of the spectral features and the spectral resolution, etc.), as the fit error underestimates the true measurement error (Stutz and Platt, 1996), depending on the number of absorption bands, the number of channels used for evaluation, the intensity of the recorded spectrum, uncertainties in the wavelength-pixel mapping and the scale and structures in the residual spectrum. The values are derived for measurements with relative high trace gas concentration. Thus, measurement error and detection limit may actually be lower for lower concentrations due to weaker structures in the residual spectrum. The relative error decreases with higher concentrations. But at higher concentration larger residual structures arise due to imperfect description of the absorption bands. Thus, the absolute error and detection limit increase. The detection limit is given as twice the 1σ measurement error.

Example fits of different trace gases are shown in Figs. 5, 6, 7 and 8. The fit result in Fig. 5 shows an example where ozone and BrO were detected simultaneously, whereas only one absorber was present in the other examples (Figs. 6–8). Compared to the measurements where only single absorbers were evaluated, the first example (Fig. 5) shows an approximately twice as large residual. This is typical for DOAS measurements, however, detection and identification of the different absorbers is possible with sufficient sensitivity. The larger measurement error in these cases is considered in the reported in the following data.

In Table 5 the detection limits for the measured trace gases for the two different mirror sets and different integration times are given. Based on the theory of Fiedler et al. (2007) we expected a better detection limit for the lower reflectivity of $R_2 = 0.99840 \pm 0.00005$ of M_2 than for M_1 ($R_1 = 0.99910 \pm 0.00009$). However we ob-

Title Page

Abstract

Introduction

Conclusions

References

Tables

Figures

◀

▶

◀

▶

Back

Close

Full Screen / Esc

Printer-friendly Version

Interactive Discussion



[Title Page](#)[Abstract](#)[Introduction](#)[Conclusions](#)[References](#)[Tables](#)[Figures](#)[Back](#)[Close](#)[Full Screen / Esc](#)[Printer-friendly Version](#)[Interactive Discussion](#)

served a better detection limit for M_1 compared to M_2 . The reason is that in practice the detection limit of a DOAS-measurement is not only dependent on the photon noise, but also on spectral structures, which are not constant in time. Other sources increasing the noise are contributions from electronic noise and optical noise e.g. additional noise introduced by the LED light source, optical fibers and spatial inhomogeneity of the optical grating of the spectrograph.

4.3 Instrument comparison

The BrO correlation plot (Fig. 10) shows a very good agreement between the CE-DOAS and the WS-DOAS systems for mixing ratios from below the respective detection limits up to 400 ppt; The slope of the BrO mixing ratios measured by each instrument is 1.06 ± 0.07 using a bivariate weighted fit as suggested by Cantrell (2008) to obtain a correlation coefficient of $r^2 = 0.95$. The agreement of HCHO of the two multi-reflection systems is remarkably good as well, with $r^2 = 0.998$ and a slope of 0.97 ± 0.03 for values up to 1 ppb using again the bivariate fit (Fig. 11). The correlation plot for ozone furthermore shows (Fig. 12) a very good agreement between the CE-DOAS and the CL-ozone monitor with a slope of 1.11 ± 0.08 and $r^2 = 0.92$, even though the CE-DOAS measurement spectral range was not optimized for ozone measurements. The excellent agreement between the two multi-reflection systems (WS and CE-DOAS), measuring at different light paths, demonstrates the accuracy and reliability of the newly developed CE-DOAS instrument. Integrity of operation is evident by the good agreement with the ozone monitor, which takes in air from a single location close to the chamber wall. This intercomparison of the instruments also demonstrates the rapid mixing of the chamber air within a timescale of 120 s (average time resolution of the instruments). A well mixed chamber is crucial for an understanding of the mechanistic of halogen release processes using chamber studies. A time series of a bromine explosion event with BrO mixing ratios of up to 360 ± 10 ppt is shown in Fig. 13. In the presence of high ozone mixing ratios of up to 350 ppb within the initial 30 min of the experiments, before the light was switched on, the BrO mixing ratio measured by the two DOAS instruments

BrO CE-DOAS

D. J. Hoch et al.

[Title Page](#)[Abstract](#)[Introduction](#)[Conclusions](#)[References](#)[Tables](#)[Figures](#)[⏪](#)[⏩](#)[◀](#)[▶](#)[Back](#)[Close](#)[Full Screen / Esc](#)[Printer-friendly Version](#)[Interactive Discussion](#)

drops to slightly negative values (around -25 ppt on average). This negative offset are probably due to interference effects, which might not be captured by the DOAS evaluation, as well as an imperfect ozone literature reference spectrum. However, the values of BrO are not significant within the 2σ measurement error of 54 ppt. The heterogeneous formation of bromine caused a total ozone depletion of 320 ppb within 150 min. The very good detection limit of the CE-DOAS compared to the White system will allow to perform chamber studies close to natural BrO levels, which are typically in the range of 200 ppt of several ppt up to more than 200 ppt (Saiz-Lopez and von Glasow, 2012).

5 Conclusions

We developed the first LED based CE-DOAS for detection of BrO in the UV-wavelength-range from 325 to 365 nm. Due to the low power consumption of the light source, the instrument can be applied to field measurements with limited power supply. The achieved BrO detection limit is 11 ppt using a time resolution of 81 min per measurement. Besides BrO also HONO, HCHO, O₃ as well as O₄ were detected in this wavelength-range. The detection limits were 450 ppt for HONO, 5.1 ppb for HCHO, and 59 ppb for O₃. The advantage of the new UV LED CE DOAS is that it is capable to measure different species (e.g. BrO, O₃ and HONO) simultaneously and with little interference. Additionally it is a remote sensing instrument and thus measuring the trace gases in comparison to most other in-situ instruments directly in the atmosphere without any losses or reactions on inlets, filters or walls. The detection limits are more than adequate for simulation-chamber measurements, where BrO levels up to 6000 ppt were observed (Buxmann et al., 2012; Ofner et al., 2012). Additionally, the instrument can improve BrO measurements of chamber experiments due to its better accuracy than state of the art DOAS White systems, which have BrO detection limits around 50 ppt (Buxmann et al., 2012).

BrO CE-DOAS

D. J. Hoch et al.

Title Page

Abstract

Introduction

Conclusions

References

Tables

Figures

◀

▶

◀

▶

Back

Close

Full Screen / Esc

Printer-friendly Version

Interactive Discussion



The relative dependence of the path length on the wavelength was determined using the absorption structures of O_3 and HONO. With an additional O_4 measurement at a known O_2 concentration, we calculated the absolute optical path length. Combining these data with the relative path length the absolute wavelength dependent mirror reflectivity and path length over the whole wavelength-range was derived. We used two sets of mirrors with different maximal reflectivity values at 347 nm, M_1 with $R_1 = 0.99910 \pm 0.00009$ ($T = 0.05\%$) and M_2 with $R_2 = 0.99840 \pm 0.00005$ ($T = 0.12\%$). We determined the absorption for both mirror sets to be in the range of 4×10^{-4} at 347 nm. The absorption is increasing towards shorter wavelengths, so that the peak of the reflectivity is shifted towards larger wavelengths compared to the transmission of the mirrors.

In contrast to expectation from the theory of Fiedler et al. (2007) we found a better detection limit for the higher reflectivity of M_1 than of M_2 . The reason is that the detection limit of a DOAS-measurement is not only dependent on the photon noise, but also on spectral structures which are not constant in time. Other sources for increasing noise are electronic noise and optical noise originating e.g. from the LED light source, optical fibers and spatial inhomogeneity of the optical grating of the spectrograph.

Several options are possible for improvement of the system in the future: mirrors with higher reflectivity lead to lower detection limits, if the absorption of the mirrors can be reduced (e.g. by using different materials during the production process, which is currently under development by different companies). With the current absorptions, a higher reflectivity will not result in much lower detection limits. The base path length could also be expanded, but at the expense of compactness and ease of handling of the instrument set up. For most measurements this is not applicable.

Another aim is to increase the light intensity for a better time resolution and therefore improved detection limit. The intensity of UV-LEDs is still very poor, but its improvement is a topic of current research at all LED manufacturers. Cooling of the LED looks also promising, since cooling of 30 K down to -10°C was found to increase the radiation intensity up to 50% (for an LED operation current of 1 mA) as expected from the data

BrO CE-DOAS

D. J. Hoch et al.

Title Page

Abstract

Introduction

Conclusions

References

Tables

Figures



Back

Close

Full Screen / Esc

Printer-friendly Version

Interactive Discussion



sheet (SET, 2010). While this work demonstrates that CE-DOAS measurements are feasible applying UV-LEDs as a light source, it is noted that xenon arc lamps may provide a 450 times higher input radiance. When compared to the electrical input, however, both devices deliver a similar radiance per input power. Therefore, UV-LEDs may present a competitive alternative light source to xenon arc lamps depending on the application of the presented instrument.

Furthermore, the system could be improved with a spectrometer with higher light throughput and larger entrance slit area to use more of the radiation exiting the cavity. Finally, we expect improvement of the detection limit from reduced optical noise. Our new UV-LED CE-DOAS is a new prototype instrument. Applying the above improvements and assuming that UV LED development will continue in the near future we expect that accuracy and detection limit of the instrument can be improved by an order of magnitude during the next few years.

For validation an intercomparison between the CE-DOAS and a WS DOAS as well as between the CE-DOAS and a chemiluminescence-ozone monitor was performed. Excellent agreement between the two multi-reflection systems (WS and CE-DOAS), measuring at different light paths and good agreement with the CL-ozone monitor was achieved. This demonstrates the reliability of the newly designed CE-DOAS instrument.

Due to its compact size and low power consumption it is possible to apply the BrO CE-DOAS-instrument – besides in reaction chamber investigations – also in field studies with batteries even if other electrical power is not available. To to our knowledge this instrument is the first mobile cavity based BrO instrument in the UV wavelength range, which is applicable to field measurements. As mentioned above two other CE-instruments exist for the detection of BrO (Chen and Venables, 2011; Grilli et al., 2012), but their field application seems to be limited due to size and power consumption.

Furthermore, BrO instruments with inlets, like CIMS (e.g. Liao et al., 2011) and mode-locked frequency-double CE-spectrometer (Grilli et al., 2012) suffer from the problem of inlet losses. For the later it was even not well characterized. Our novel UV-CE-DOAS instrument provides a very good alternative, as it is an open path in-

BrO CE-DOAS

D. J. Hoch et al.

Title Page

Abstract

Introduction

Conclusions

References

Tables

Figures

◀

▶

◀

▶

Back

Close

Full Screen / Esc

Printer-friendly Version

Interactive Discussion



strument without any inlets, and the self-calibrating DOAS retrieval is used. We like to stress, that there are several areas where BrO has been detected in the atmosphere at levels exceeding the detection limit of the presented version of our CE-DOAS instrument, e.g. in arctic regions 41 ppt (Pöhler et al., 2010), at the Salar de Uyuni, Bolivia up to 20 ppt (Hönninger et al., 2004), at the Dead Sea 200 ppt (Hebestreit et al., 1999; Matveev et al., 2001; Tas et al., 2008), or in volcanic plumes, where BrO mixing ratios of the order of 1000 ppt were inferred (Bobrowski et al., 2003). All these observations are averaged concentrations over few km long light paths. Thus the BrO CE-DOAS instrument can help to study the involved processes by deriving in-situ BrO concentrations which are probably even higher. Moreover, it appears likely that the detection limits of our instrument can be greatly improved in the future.

Acknowledgements. We are grateful to the German Science Foundation (DFG) for funding the research unit 763, HALOPROC, to H.-U. Krüger (deceased) for technical support, to M. Sörgel for generation of HONO and to J. Ofner, S. Bleicher, and N. Balzer for helping with the chemical tasks.

References

- Ball, S. M. and Jones, R. L.: Broad-Band Cavity Ring-Down Spectroscopy, *Chem. Rev.*, 103, 5239–5262, 2003. 6049
- Ball, S. M., Povey, I. M., Norton, E. G., and Jones, R. L.: Broadband cavity ringdown spectroscopy of the NO₃ radical, *Chem. Phys. Lett.*, 342, 113–120, 2001. 6049
- Ball, S. M., Langridge, J., and Jones, R.: Broadband cavity enhanced absorption spectroscopy using light emitting diodes, *Chem. Phys. Lett.*, 398, 68–74, 2004. 6050, 6053
- Barrie, L. A., Bottenheim, J., Schnell, R., Crutzen, P., and Rasmussen, R.: Ozone destruction and photochemical reactions at polar sunrise in the lower Arctic atmosphere, *Nature*, 334, 138–141, 1988. 6049
- Barrie, L. A., Bottenheim, J. W., and Hart, W. R.: Polar Sunrise Experiment 1992 (PSE 1992): Preface, *J. Geophys. Res.*, 99, 25313–25314, 1994. 6049

[Title Page](#)[Abstract](#)[Introduction](#)[Conclusions](#)[References](#)[Tables](#)[Figures](#)[⏪](#)[⏩](#)[◀](#)[▶](#)[Back](#)[Close](#)[Full Screen / Esc](#)[Printer-friendly Version](#)[Interactive Discussion](#)

Bleicher, S.: Halogenaktivierung im Aerosol und Salzpflanzen -Experimente und Modellierung in einer Umweltkammer, Ph.D. thesis, Atmospheric Chemistry Research Laboratory, University of Bayreuth, Bayreuth, Germany, 2012. 6063, 6064

Bobrowski, N., Hönniger, G., Galle, B., and Platt, U.: Detection of Bromine Monoxide in a Volcanic Plume, *Nature*, 423, 273–276, 2003. 6071

Bottenheim, J. W., Gallant, A. C., and Brice, K.: Measurements of NO_y species and O₃ at 82° N latitude, *Geophys. Res. Lett.*, 13, 113–116, 1986. 6048

Bottenheim, J. W., Barrie, L. A., Atlas, E., Heidt, L. E., Niki, H., Rasmussen, R. A., and Shepson, P. B.: Depletion of lower tropospheric ozone during Arctic spring: The polar sunrise experiment 1988, *J. Geophys. Res.*, 95, 18555–18568, 1990. 6049

Buxmann, J.: “Bromine and Chlorine Explosion” in a simulated Atmosphere, Ph.D. thesis, Institute of Environmental Physics, University of Heidelberg, Heidelberg, Germany, 2012. 6064

Buxmann, J., Balzer, N., Bleicher, S., Platt, U., and Zetzsch, K.: Observations of bromine explosions in smog chamber experiments above a model salt pan, *Int. J. Chem. Kinet.*, 44, 312–326, doi:10.1002/kin.20714, 2012. 6049, 6063, 6064, 6068

Cantrell, C. A.: Technical Note: Review of methods for linear least-squares fitting of data and application to atmospheric chemistry problems, *Atmos. Chem. Phys.*, 8, 5477–5487, doi:10.5194/acp-8-5477-2008, 2008. 6067

Chen, J. and Venables, D. S.: A broadband optical cavity spectrometer for measuring weak near-ultraviolet absorption spectra of gases, *Atmos. Meas. Tech.*, 4, 425–436, doi:10.5194/amt-4-425-2011, 2011. 6050, 6070

Chen, J., Wenger, J., and Venables, D.: Near-ultraviolet absorption cross sections of nitrophenols and their potential influence on tropospheric oxidation capacity, *J. Phys. Chem. A*, 115, 12235–12242, doi:10.1021/jp206929r, 2011. 6050

Engeln, R., Berden, G., Peeters, R., and Meijer, G.: Cavity enhanced absorption and cavity enhanced magnetic rotation spectroscopy, *Rev. Sci. Instrum.*, 69, 3763–3769, 1998. 6050

Fawcett, B. L., Parkes, A. M., Shallcross, D. E., and Orr-Ewing, A. J.: Trace detection of methane using continuous wave cavity ring-down spectroscopy at 1.65 μm, *Phys. Chem. Chem. Phys.*, 4, 5960–5965, 2002. 6049

Fiedler, S., Hese, A., and Ruth, A. A.: Incoherent broad-band cavity-enhanced absorption spectroscopy, *Chem. Phys. Lett.*, 371, 284–294, doi:10.1016/S0009-2614(03)00263-X, 2003. 6050

BrO CE-DOAS

D. J. Hoch et al.

Title Page

Abstract

Introduction

Conclusions

References

Tables

Figures

◀

▶

◀

▶

Back

Close

Full Screen / Esc

Printer-friendly Version

Interactive Discussion



- Fiedler, S., Hese, A., and Heitmann, U.: Influence of the cavity parameters on the output intensity in incoherent broadband cavity-enhanced absorption spectroscopy, *Rev. Sci. Instrum.*, 78, 073104, doi:10.1063/1.2752608, 2007. 6058, 6065, 6066, 6069, 6087
- 5 Fleischmann, O. C. and Burrows, J.: New ultraviolet absorption cross-sections of BrO at atmospheric temperatures measured by time-windowing fourier transform spectroscopy, *J. Photochem. Photobiol. A*, 168, 117–132, 2004. 6081
- Friess, U., Sihler, H., Sander, R., Poehler, D., Yilmaz, S., and Platt, U.: The vertical distribution of BrO and aerosols in the Arctic: Measurements by active and passive differential optical absorption spectroscopy, *J. Geophys. Res.-Atmos.*, 116, D00R04, doi:10.1029/2011JD015938, 10 2011. 6049
- Gherman, T., Venables, D. S., Vaughan, S., Orphal, J., and Ruth, A. A.: Incoherent broadband cavity-enhanced absorption spectroscopy in the near-ultraviolet: application to HONO and NO₂, *Environ. Sci. Technol.*, 42, 820–895, 2008. 6050
- 15 Greenblatt, G. D., Orlando, J. J., Burkholder, J. B., and Ravishankara, A. R.: Absorption measurements of oxygen between 330 and 1140 nm, *J. Geophys. Res.-Atmos.*, 95, 18577–18582, 1990. 6081
- Grilli, R., Mejean, G., Kassi, S., Ventrillard, I., Abd-Alrahman, C., Fasci, E., and Romanini, D.: Trace measurement of BrO at the ppt level by a transportable mode-locked frequency-doubled cavity-enhanced spectrometer, *Appl. Phys. B*, 107, 205–212, doi:10.1007/s00340-011-4812-9, 2012. 6050, 6051, 6070
- 20 Hausmann M. and Platt U.: Spectroscopic measurement of bromine oxide and ozone in the high Arctic during Polar Sunrise Experiment 1992, *J. Geophys. Res.*, 99, 25399-25413. 1994. 6049
- Hak, C., Pundt, I., Trick, S., Kern, C., Platt, U., Dommen, J., Ordóñez, C., Prévôt, A. S. H., Junkermann, W., Astorga-Lloréns, C., Larsen, B. R., Mellqvist, J., Strandberg, A., Yu, Y., Galle, B., Kleffmann, J., Lörzer, J. C., Braathen, G. O., and Volkamer, R.: Intercomparison of four different in-situ techniques for ambient formaldehyde measurements in urban air, *Atmos. Chem. Phys.*, 5, 2881–2900, doi:10.5194/acp-5-2881-2005, 2005. 6063
- 25 Hebestreit, K., Stutz, J., Rosen, D., Matveiv, V., Peleg, M., Luria, M., and Platt, U.: DOAS measurements of tropospheric bromine oxide in mid-latitudes, *Science*, 283, 55–57, 1999. 6049, 6071
- 30 Hoch, D. J.: Resonator Verstärkte Differentielle Optische Absorptions Spektroskopie: Labormessungen von BrO, HCHO, HONO und O₃, Diploma thesis, Inst. for Environmen-

BrO CE-DOAS

D. J. Hoch et al.

Title Page

Abstract

Introduction

Conclusions

References

Tables

Figures

◀

▶

◀

▶

Back

Close

Full Screen / Esc

Printer-friendly Version

Interactive Discussion



tal Physics (IUP), Atmosphere and Remote Sensing, Ruprecht-Karls-Universität Heidelberg, Heidelberg, Germany, 2010. 6056

Hönninger, G., Bobrowski, N., Palenque, E., Torrez, R., and Platt, U.: Reactive bromine and sulfur emissions at Salar de Uyuni, Bolivia, *Geophys. Res. Lett.*, 31, L04101, doi:10.1029/2003GL018818, 2004. 6049, 6071

Horbanski, M.: A Compact Resonator Based Instrument for DOAS Measurements of Ambient Nitrogen Dioxide, Diploma thesis, Inst. for Environmental Physics – IUP, Atmosphere and Remote Sensing, University of Heidelberg, Heidelberg, Germany, 2010. 6054

Horbanski, M., Pöhler, D., and Platt, U.: iCE-DOAS: A new iterative evaluation algorithm for compact and light weight resonator based DOAS instruments, in preparation, 2013. 6054

Kahan, T. F., Washenfelder, R. A., Vaida, V., and Brown, S. S.: Cavity-enhanced measurements of hydrogen peroxide absorption cross sections from 353 to 410 nm, *J. Phys. Chem. A*, 116, 5941–5947, doi:10.1021/jp2104616, 2012. 6050

Kern, C., Trick, S., Rippel, B., and Platt, U.: Applicability of light-emitting diodes as light sources for active DOAS measurements, *Appl. Optics*, 45, 2077–2088, 2006. 6057

Kraus, S.: DOASIS: DOAS Intelligent System, Software, copyright 2004 Stefan Kraus, Institute of Environmental Physics, University of Heidelberg, Germany, in cooperation with Hoffmann Messtechnik GmbH, 2004. 6059, 6064

Kreher, K., Johnston, P. V., Wood, S. W., and Platt, U.: Ground-based measurements of tropospheric and stratospheric BrO at Arrival Heights, Antarctica, *Geophys. Res. Lett.*, 24, 3021–3024, doi:10.1029/97GL02997, 1997. 6049

Langridge, J. M., Ball, S. M., and Jones, R. L.: A compact broadband cavity enhanced absorption spectrometer for detection of atmospheric NO₂ using light emitting diodes, *Analyst*, 131, 916–922, 2006. 6050

Langridge, J. M., Laurila, T., Watt, R. S., Jones, R. L., Kaminski, C. F., and Hult, J.: Cavity enhanced absorption spectroscopy of multiple trace gas species using a supercontinuum radiation source, *Opt. Express*, 16, 10178–10188, 2008. 6050

Leser, H., Hönninger, G., and Platt, U.: MAX-DOAS measurements of BrO and NO₂ in the marine boundary layer, *Geophys. Res. Lett.*, 30, 1537, doi:10.1029/2002GL015811, 2003. 6049

Liao, J., Sihler, H., Huey, L. G., Neuman, J. A., Tanner, D. J., Friess, U., Platt, U., Flocke, F. M., Orlando, J. J., Shepson, P. B., Beine, H. J., Weinheimer, A. J., Sjostedt, S. J., Nowak, J. B., Knapp, D. J., Staebler, R. M., Zheng, W., Sander, R., Hall, S. R., and Ullmann,

BrO CE-DOAS

D. J. Hoch et al.

Title Page

Abstract

Introduction

Conclusions

References

Tables

Figures

◀

▶

◀

▶

Back

Close

Full Screen / Esc

Printer-friendly Version

Interactive Discussion



K.: A comparison of Arctic BrO measurements by chemical ionization mass spectrometry and long path-differential optical absorption spectroscopy, *J. Geophys. Res.*, 116, D00R02, doi:10.1029/2010JD014788, 2011. 6050, 6051, 6070

5 Mahajan, A. S., Plane, J. M. C., Oetjen, H., Mendes, L., Saunders, R. W., Saiz-Lopez, A., Jones, C. E., Carpenter, L. J., and McFiggans, G. B.: Measurement and modelling of tropospheric reactive halogen species over the tropical Atlantic Ocean, *Atmos. Chem. Phys.*, 10, 4611–4624, doi:10.5194/acp-10-4611-2010, 2010. 6049

10 Matveev, V., Peleg, M., Rosen, D., Tov-Alper, D. S., Hebestreit, K., Stutz, J., Platt, U., Blake, D., and Luria, M.: Bromine oxide – ozone interaction over the Dead Sea, *J. Geophys. Res.*, 106, 10375–10387, 2001. 6049, 6071

Meinen, J., Thieser, J., Platt, U., and Leisner, T.: Technical Note: Using a high finesse optical resonator to provide a long light path for differential optical absorption spectroscopy: CE-DOAS, *Atmos. Chem. Phys.*, 10, 3901–3914, doi:10.5194/acp-10-3901-2010, 2010. 6050, 6052, 6053, 6060

15 Meller, R. and Moortgat, G.: Temperature dependence of the absorption cross sections of formaldehyde between 223 and 323 K in the wavelength range 225–375 nm, *J. Geophys. Res.-Atmos.*, 105, 7089–7101, 2000. 6081

20 Neuman, J. A., Nowak, J. B., Huey, L. G., Burkholder, J. B., Dibb, J. E., Holloway, J. S., Liao, J., Peischl, J., Roberts, J. M., Ryerson, T. B., Scheuer, E., Stark, H., Stickel, R. E., Tanner, D. J., and Weinheimer, A.: Bromine measurements in ozone depleted air over the Arctic Ocean, *Atmos. Chem. Phys.*, 10, 6503–6514, doi:10.5194/acp-10-6503-2010, 2010. 6050, 6051

25 Ofner, J., Balzer, N., Buxmann, J., Grothe, H., Schmitt-Kopplin, Ph., Platt, U., and Zetzsch, C.: Halogenation processes of secondary organic aerosol and implications on halogen release mechanisms, *Atmos. Chem. Phys.*, 12, 5787–5806, doi:10.5194/acp-12-5787-2012, 2012. 6049, 6068

O’Keefe, A. and Deacon, D.: Cavity ring-down optical spectrometer for absorption measurements using pulsed laser sources, *Rev. Sci. Instrum.*, 59, 2544–2551, doi:10.1063/1.1139895, 1988. 6049

30 Orphal, J. and Ruth, A. A.: High-resolution Fourier-transform cavity-enhanced absorption spectroscopy in the near-infrared using an incoherent broad-band light source, *Opt. Express*, 16, 19232–19243, 2008. 6050

OSRAM: XBO 75W/2 Product datasheet, available at: , last access: 7 May 2013. 6057

[Title Page](#)[Abstract](#)[Introduction](#)[Conclusions](#)[References](#)[Tables](#)[Figures](#)[◀](#)[▶](#)[◀](#)[▶](#)[Back](#)[Close](#)[Full Screen / Esc](#)[Printer-friendly Version](#)[Interactive Discussion](#)

- Paldus, B. A., Harb, C. C., Spence, T. G., Zare, R. N., Gmachl, C., Capasso, F., Sivco, D. L., Baillargeon, J. N., Hutchinson, A. L., and Cho, A. Y.: Cavity ringdown spectroscopy using mid-infrared quantum-cascade lasers, *Opt. Express*, 25, 666–668, 2000. 6049
- Peeters, R., Berden, G., Apituley, A., and Meijer, G.: Open-path trace gas detection of ammonia based on cavity-enhanced absorption spectroscopy, *Appl. Phys. B*, 71, 231–236, 2000. 6050
- Pöhler, D., Vogel, L., Friess, U., and Platt, U.: Observation of halogen species in the Amundsen Gulf, Arctic, by active long-path differential optical absorption spectroscopy, *P. Natl. Acad. Sci. USA*, 107, 6582–6587, 2010. 6049, 6071
- Platt, U. and Lehrer, E.: Arctic Tropospheric Ozone Chemistry, ARCTOC, Final Report of the EU-Project No. EV5V-CT93-0318, Heidelberg, 1996. 6049
- Platt, U. and Stutz, J.: *Differential Optical Absorption Spectroscopy: Principles and Applications*, Physics of Earth and Space Environments, Springer-Verlag, Berlin, Heidelberg, 2008. 6050, 6053
- Platt, U., Meinen, J., Pöhler, D., and Leisner, T.: Broadband Cavity Enhanced Differential Optical Absorption Spectroscopy (CE-DOAS) – applicability and corrections, *Atmos. Meas. Tech.*, 2, 713–723, doi:10.5194/amt-2-713-2009, 2009. 6050, 6053, 6054
- Read, K., Mahajan, A., Carpenter, L., Evans, M., Faria, B., Heard, D., Hopkins, J., Lee, J., Moller, S., Lewis, A., Mendes, L., McQuaid, J., Oetjen, H., Saiz-Lopez, A., Pilling, M., and Plane, J.: Extensive halogen-mediated ozone destruction over the tropical Atlantic Ocean, *Nature*, 453, 1232–1235, doi:10.1038/nature07035, 2008. 6049
- Ritz, D., Hausmann, M., and Platt, U.: An improved open path multi-reflection cell for the measurement of NO₂ and NO₃, in: *Optical Methods in Atmospheric Chemistry*, edited by: Schiff, H. I. and Platt, U., Proc. SPIE, 1715, 200–211, doi:10.1117/12.140211, 1993. 6063
- Saiz-Lopez, A. and von Glasow, R.: Reactive halogen chemistry in the troposphere, *Chem. Soc. Rev.*, 2012, 6448–6472, doi:10.1039/C2CS35208G, 2012. 6068
- Saiz-Lopez, A., Plane, J. M. C., and Shillito, J. A.: Bromine oxide in the mid-latitude marine boundary layer, *Geophys. Res. Lett.*, 31, L03111, doi:10.1029/2003GL018956, 2004. 6049
- Saiz-Lopez, A., Mahajan, A. S., Salmon, R. A., Bauguitte, S. J.-B., Jones, A. E., Roscoe, H. K., and Plane, J. M. C.: Boundary layer halogens in coastal Antarctica, *Science*, 317, 348–352, doi:10.1126/science.1141408, 2007. 6049
- Schuster, G., Labazan, I., and Crowley, J. N.: A cavity ring down/cavity enhanced absorption device for measurement of ambient NO₃ and N₂O₅, *Atmos. eas. Tech.*, 2, 1–13, doi:10.5194/amt-2-1-2009, 2009. 6049

- SET: UVTOP Technical Data, available at: <http://www.s-et.com> (last access: 23 April 2012), 2010. 6057, 6070
- Siekmann, F.: Freisetzung von photolabilen und reaktiven Halogenverbindungen aus salzhaltigen Aerosolen unter simulierten und troposphärischen Reinluftbedingungen in einer Aerosol-Smogkammer, Ph.D. thesis, Atmospheric Chemistry Research Laboratory, University of Bayreuth, Bayreuth, Germany, 2008. 6063
- 5 Sihler, H., Kern, C., Pöhler, D., and Platt, U.: Applying light-emitting diodes with narrowband emission features in differential spectroscopy, *Opt. Lett.*, **34**, 3716–3718, 2009. 6057
- Simpson, W. R.: Continuous wave cavity ring-down spectroscopy applied to in situ detection of dinitrogen pentoxide (N_2O_5), *Rev. Sci. Instrum.*, **74**, 3442–3452, 2003. 6049
- 10 Sturges, W. T., Schnell, R. C., Landsberger, S., Oltmans, S. J., Harris, J. M., and Li, S.-M.: Chemical and meteorological influences on surface ozone destruction at Barrow, Alaska, during spring 1989, *Atmos. Environ.*, **27A**, 2851–2863, 1993. 6049
- Stutz, J. and Platt, U.: Numerical analysis and estimation of the statistical error of differential optical absorption spectroscopy measurements with least-squares methods, *Appl. Opt.*, **35**, 6041–6053, doi:10.1364/AO.35.006041, 1996. 6065, 6066
- 15 Stutz, J., Kim, E., Platt, U., Bruno, P., Perrino, C., and Febo, A.: UV-visible absorption cross section of nitrous acid, *J. Geophys. Res.-Atmos.*, **105**, 14585–14592, 2000. 6081
- Taira, M. and Kanda, Y.: Continuous generation system for low-concentration gaseous nitrous acid, *Anal. Chem.*, **62**, 630–633, doi:10.1021/ac00205a018, 1990. 6062
- 20 Tas, E., Peleg, M., Pedersen, D. U., Matveev, V., Biazar, A. P., and Luria, M.: Measurement-based modeling of bromine chemistry in the Dead Sea boundary layer – Part 2: The influence of NO_2 on bromine chemistry at mid-latitude areas, *Atmos. Chem. Phys.*, **8**, 4811–4821, doi:10.5194/acp-8-4811-2008, 2008. 6049, 6071
- 25 Thalman, R. and Volkamer, R.: Inherent calibration of a blue LED-CE-DOAS instrument to measure iodine oxide, glyoxal, methyl glyoxal, nitrogen dioxide, water vapour and aerosol extinction in open cavity mode, *Atmos. Meas. Tech.*, **3**, 1797–1814, doi:10.5194/amt-3-1797-2010, 2010. 6050
- Tuckermann, M., Ackermann, R., Golz, C., Lorenzen Schmidt, H., Senne, T., Stutz, J., Trost, B., Unold, W., and Platt, U.: DOAS-observation of halogen radical-catalysed arctic boundary layer ozone destruction during the ARCTOC-campaigns 1995 and 1996 in Ny-Alesund, Spitsbergen, *Tellus B*, **49**, 533–555, doi:10.1034/j.1600-0889.49.issue5.9.x, 1997. 6049
- 30

[Title Page](#)[Abstract](#)[Introduction](#)[Conclusions](#)[References](#)[Tables](#)[Figures](#)[◀](#)[▶](#)[◀](#)[▶](#)[Back](#)[Close](#)[Full Screen / Esc](#)[Printer-friendly Version](#)[Interactive Discussion](#)

BrO CE-DOAS

D. J. Hoch et al.

[Title Page](#)[Abstract](#)[Introduction](#)[Conclusions](#)[References](#)[Tables](#)[Figures](#)[◀](#)[▶](#)[◀](#)[▶](#)[Back](#)[Close](#)[Full Screen / Esc](#)[Printer-friendly Version](#)[Interactive Discussion](#)

- Varma, R. M., Venables, D. S., Ruth, A. A., Heitmann, U., Schlosser, E., and Dixneuf, S.: Long optical cavities for open-path monitoring of atmospheric trace gases and aerosol extinction, *Appl. Optics*, 48, B159–B171, 2009. 6050
- 5 Vaughan, S., Gherman, T., Ruth, A. A., and Orphal, J.: Incoherent broad-band cavity-enhanced absorption spectroscopy of the marine boundary layer species I-2, IO and OIO, *Phys. Chem. Chem. Phys.*, 10, 4471–4477, 2008. 6050
- Venables, D., Gherman, T., Orphal, J., Wenger, J., and Ruth, A.: High sensitivity in situ monitoring of NO₃ in an atmospheric simulation chamber using incoherent broadband cavity-enhanced absorption spectroscopy, *Environ. Sci. Technol.*, 40, 6758–6763, 2006. 6050, 6056
- 10 Voigt, S., Orphal, J., Bogumil, K., and Burrows, J.: The temperature dependence (203–293 K) of the absorption cross sections of O₃ in the 230–850 nm region measured by Fourier-transform spectroscopy, *J. Photochem. Photobiol. A*, 143, 1–9, 2001. 6081
- Voigt, S., Orphal, J., and Burrows, J.: The temperature and pressure dependence of the absorption cross-sections of NO₂ in the 250–800 nm region measured by Fourier-transform spectroscopy, *J. Photochem. Photobiol. A*, 149, 1–7, 2002. 6081
- 15 Volkamer, R.: Absorption von Sauerstoff im Herzberg I System und Anwendung auf Aromatenmessungen am EUROpean PHOto REactor (EUPHORE), Diploma thesis, Institute of Environmental Physics, University of Heidelberg, Heidelberg, Germany, 1996. 6063
- 20 Volkamer, R., Junkermann, W., Wirtz, K., and Platt, U.: Formation of formaldehyde, glyoxal and methylglyoxal from the toluene + OH reaction in the presence of NO_x, poster presented at EGS XXVII General Assembly, Nice, France, 2002. 6063
- Washenfelder, R. A., Langford, A. O., Fuchs, H., and Brown, S. S.: Measurement of glyoxal using an incoherent broadband cavity enhanced absorption spectrometer, *Atmos. Chem. Phys.*, 8, 7779–7793, doi:10.5194/acp-8-7779-2008, 2008. 6050, 6053
- 25 White, J. U.: Long Paths of Large Aperture, *J. Opt. Soc. Am.*, 32, 285–288, 1942. 6063
- White, J. U.: Very long optical paths in air, *J. Opt. Soc. Am.*, 66, 411–416, 1976. 6063
- Zalicki, P. and Zare, R.: Cavity ring-down spectroscopy for quantitative absorption measurements, *J. Chem. Phys.*, 107, 2708–2717, 1995. 6049

[Title Page](#)[Abstract](#)[Introduction](#)[Conclusions](#)[References](#)[Tables](#)[Figures](#)[Back](#)[Close](#)[Full Screen / Esc](#)[Printer-friendly Version](#)[Interactive Discussion](#)**Table 1.** Chamber sizes and base-path lengths for set-ups A, B and C.

Set-up (chamber type)	Cavity length (d_0) [cm]	Absorption length (d) [cm]	Volume [l]
A (glass)	107 ± 1	47 ± 1	7.5
B (Teflon)	149 ± 1	127 ± 1	40
C (Teflon)	181 ± 1	159 ± 1	50

[Title Page](#)[Abstract](#)[Introduction](#)[Conclusions](#)[References](#)[Tables](#)[Figures](#)[Back](#)[Close](#)[Full Screen / Esc](#)[Printer-friendly Version](#)[Interactive Discussion](#)**Table 2.** Measurement set-ups for detection of different trace gases.

Measurement	Mirror set	Set-up
O ₃	<i>M</i> ₁ and <i>M</i> ₂	A
O ₃	<i>M</i> ₂	B
O ₃	<i>M</i> ₁	C
HONO	<i>M</i> ₁ and <i>M</i> ₂	A
HONO	<i>M</i> ₂	B
HONO	<i>M</i> ₁	C
BrO	<i>M</i> ₂	B
BrO	<i>M</i> ₁	C
O ₄	<i>M</i> ₁ and <i>M</i> ₂	A
O ₄	<i>M</i> ₁	C

BrO CE-DOAS

D. J. Hoch et al.

Title Page

Abstract

Introduction

Conclusions

References

Tables

Figures

◀

▶

◀

▶

Back

Close

Full Screen / Esc

Printer-friendly Version

Interactive Discussion



Table 3. Literature absorption cross sections used in the DOAS evaluation. The cross sections were corrected with a Pre-shift and linked together for the following measurements.

Trace gas	Reference	Pre-shift [nm]	Shift
BrO	Fleischmann and Burrows (2004)	0.153	free
HCHO	Meller and Moortgat (2000)	0.0018	linked to BrO
HONO	Stutz et al. (2000)	0.08221	linked to BrO
O ₄	Greenblatt et al. (1990)	0.578	linked to BrO
O ₃	Voigt et al. (2001)	0.206	linked to BrO
NO ₂	Voigt et al. (2002)	0	linked to BrO

Table 5. Mean detection limits including the presence of high ozone concentrations for different measurement configurations. Mirror set M_1 with $R_1 = 0.99910 \pm 0.00009$ and M_2 with $R_2 = 0.99840 \pm 0.00005$. The path length \bar{L}_{eff} (at 347 nm) is for setup B = 839 m and for setup C = 1472 m, with an accuracy of 2%. An estimate for the NO_2 detection limit is given.

Trace gas	Mirrors	Path length at 347 nm [m]	Integration time [min]	Det. lim. [ppt]	Integration time [min]	Det. lim. [ppt]
BrO	M_2	839	2.9	41	61.3	17
BrO	M_1	1472	4.8	20	80.8	11
HCHO	M_2	839	2.9	9100	61.3	5100
HONO	M_1	1472	4.8	970	106	450
O_3	M_1	1472	4.8	91 000	47.5	59 000
NO_2	M_2	816	2.9	3600		

Title Page

Abstract

Introduction

Conclusions

References

Tables

Figures



Back

Close

Full Screen / Esc

Printer-friendly Version

Interactive Discussion



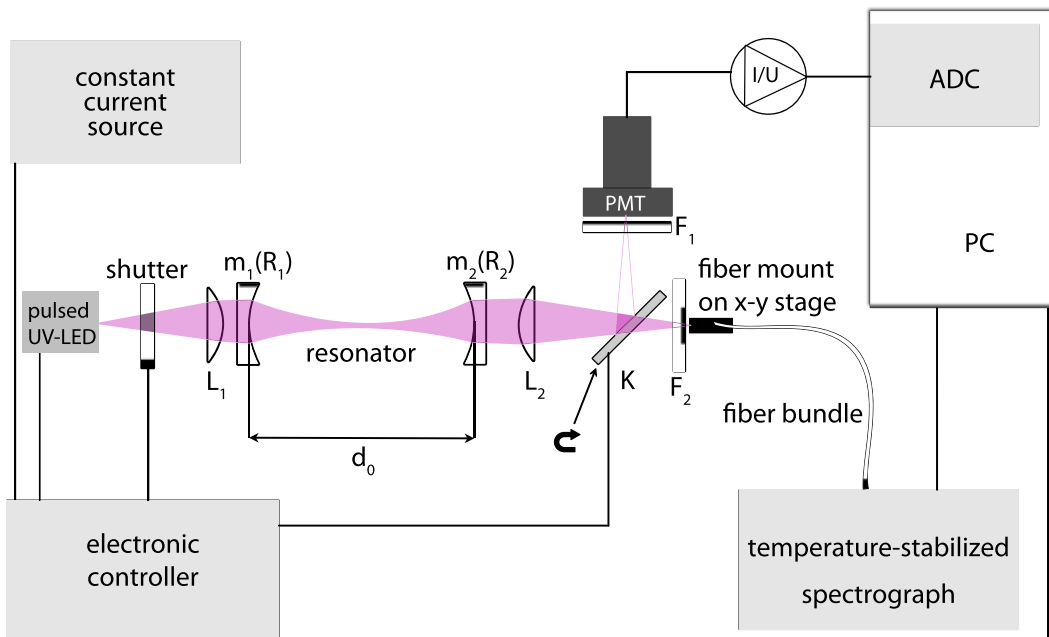


Fig. 1. Schematic diagram of the CE-DOAS-instrument. The radiation output of a pulsed UV-LED is imaged by lens L_1 into the resonator consisting of two highly reflective dielectric mirrors M_1 and M_2 . The light which leaves the resonator through M_2 is focused by the lens L_2 to a fiber bundle which is attached to a x - y stage. This fiber bundle transmits the light to a temperature stabilized spectrograph (Ocean Optics QE 65000). Alternatively the movable mirror “ K ” can redirect the light to a photomultiplier (PMT) to optionally record a ring down signal and thus check the path length of the resonator. F_1 and F_2 are band-pass filters (Schott UG11). F_1 protects the PMT and F_2 the fibers from scattered light and LED radiation outside of the reflectivity range of the mirrors. The shutter is used to perform background measurements. The electronic controller receives a constant current and creates the pulses for the UV-LED. It also controls the shutter and the mirror K .

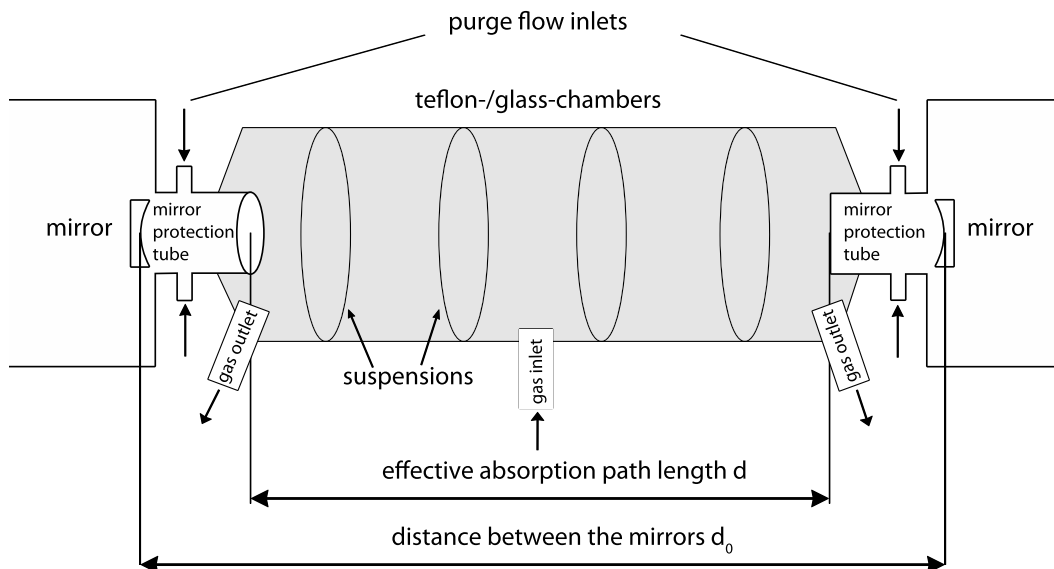


Fig. 2. Setup for the measurements at the Atmospheric Chemistry Research Laboratory, University of Bayreuth, Germany. One of three air tight chamber, made of either teflon or glass, is placed between the two mirrors. This chamber could be filled via the gas inlet with different trace gases. A purge flow of nitrogen in front of the mirrors avoids aerosols from the sample air to contaminate the mirrors. The distance between the mirrors is d_0 . The effective absorption path length is d because the sample gas only fills the volume between the ends of the mirror protection tubes between the purge gas outlets.

[Title Page](#)
[Abstract](#)
[Introduction](#)
[Conclusions](#)
[References](#)
[Tables](#)
[Figures](#)
[◀](#)
[▶](#)
[◀](#)
[▶](#)
[Back](#)
[Close](#)
[Full Screen / Esc](#)
[Printer-friendly Version](#)
[Interactive Discussion](#)

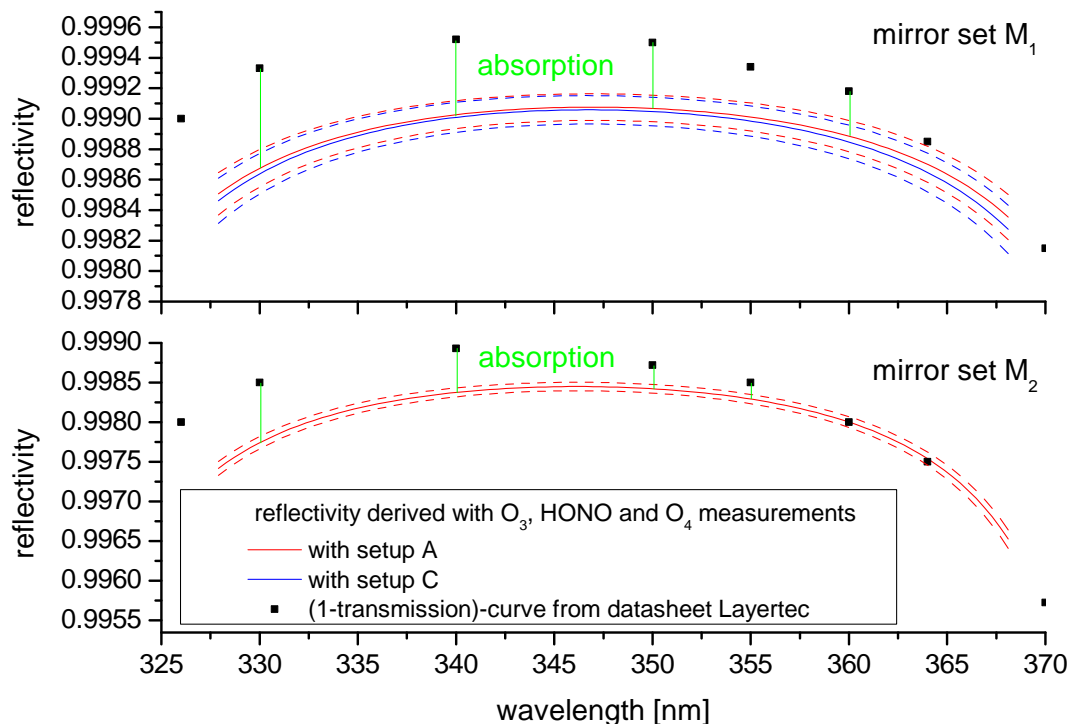



Fig. 3. Reflectivity curves of mirror sets M_1 and M_2 : the black squares indicate the (1-transmission)-curve from the manufacturer's data sheet. The red and blue lines are the reflectivities calculated from measurements with setup A and C respectively. The dashed lines are the accuracies of this determination, which are maximal 0.05% within the second-order polynomial fit range. The maximal reflectivities are $R_1 = 0.99910 \pm 0.00009$ for M_1 and $R_2 = 0.99840 \pm 0.00005$ for M_2 at 347 nm. The green lines between the black dots and the reflectivity-curves indicate the losses due to absorption in the reflective layer. It can be seen that the absorption is small at 370 nm and increases towards shorter wavelengths.

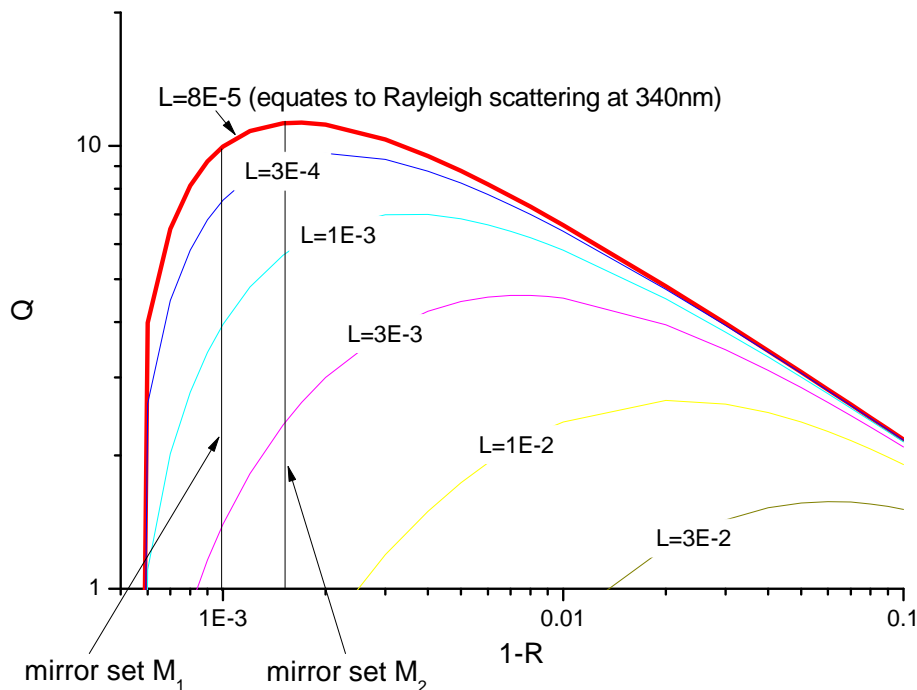


Fig. 4. Calculation of the enhancement factor (quality factor) Q from Eq. (8) (Fiedler et al., 2007) as a function of $(1 - R)$ for different losses L and a mirror absorption $A = 4 \times 10^{-4}$. The red line indicates the theoretical upper limit for Q for the minimal losses due to Rayleigh scattering in the resonator at 340 nm.



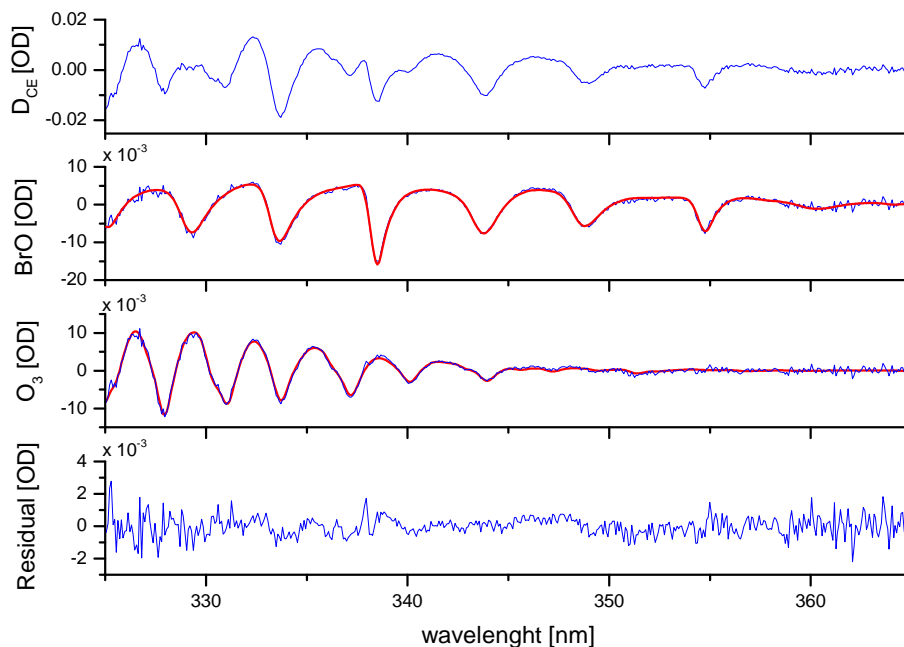


Fig. 5. Example for the spectral identification of BrO with the CE-DOAS set up. The thick red line indicates the fit result and the thin blue line the sum of the fit result and the residual. The corresponding mixing ratio for BrO is (507 ± 11) ppt and for O_3 (1984 ± 51) ppb. The residual is 4×10^{-3} peak to peak.

[Title Page](#)[Abstract](#)[Introduction](#)[Conclusions](#)[References](#)[Tables](#)[Figures](#)[◀](#)[▶](#)[◀](#)[▶](#)[Back](#)[Close](#)[Full Screen / Esc](#)[Printer-friendly Version](#)[Interactive Discussion](#)

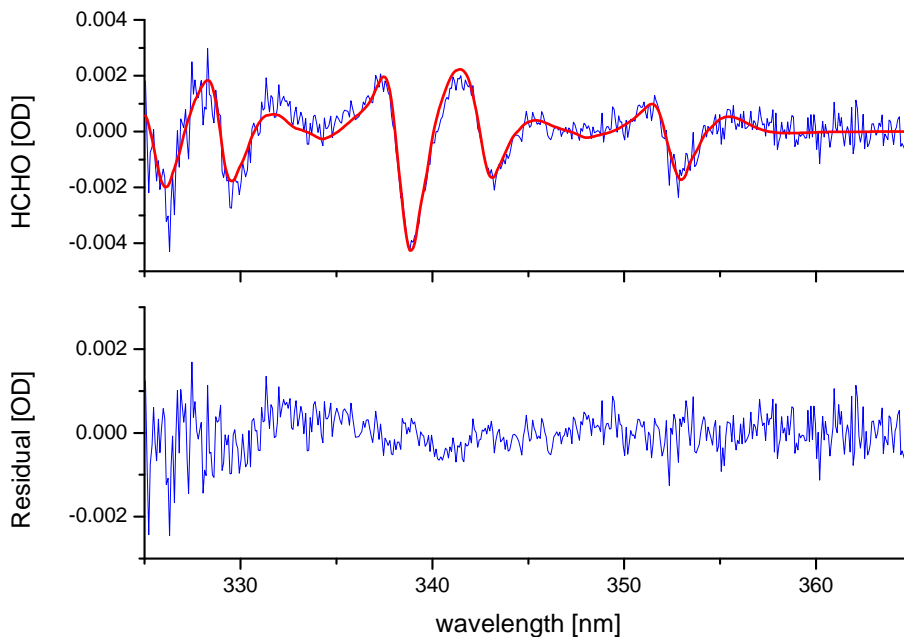


Fig. 6. Spectral DOAS fit of HCHO with (88 ± 6) ppb. Upper panel: the thick red line indicates the fit result and the thin blue line the sum of the fit result and the residual. Lower panel: fit residual with peak to peak 3×10^{-3} .

Title Page

Abstract

Introduction

Conclusions

References

Tables

Figures

⏪

⏩

◀

▶

Back

Close

Full Screen / Esc

Printer-friendly Version

Interactive Discussion



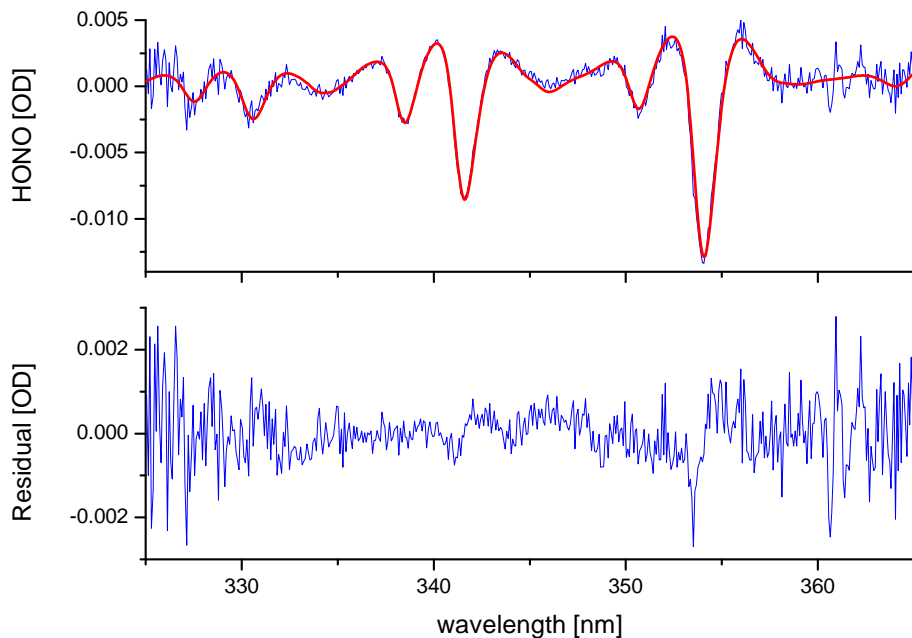


Fig. 7. Spectral DOAS fit of HONO with (16.0 ± 0.7) ppb. Upper panel: the thick red line indicates the fit result and the blue thin line the sum of the fit result and the residual. Lower panel: fit residual with peak to peak 4×10^{-3} .

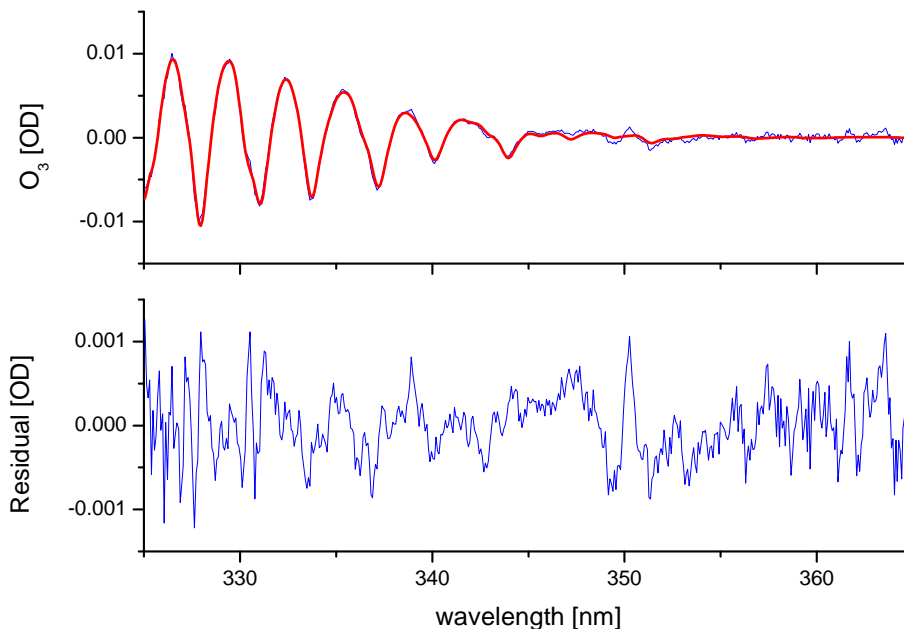


Fig. 8. Spectral DOAS fit of O₃ with (1766 ± 59) ppb. Upper panel: the thick red line indicates the fit result and the thin blue line the sum of the fit result and the residual. Lower panel: fit residual with peak to peak 2×10^{-3} .

[Title Page](#)[Abstract](#)[Introduction](#)[Conclusions](#)[References](#)[Tables](#)[Figures](#)[◀](#)[▶](#)[◀](#)[▶](#)[Back](#)[Close](#)[Full Screen / Esc](#)[Printer-friendly Version](#)[Interactive Discussion](#)

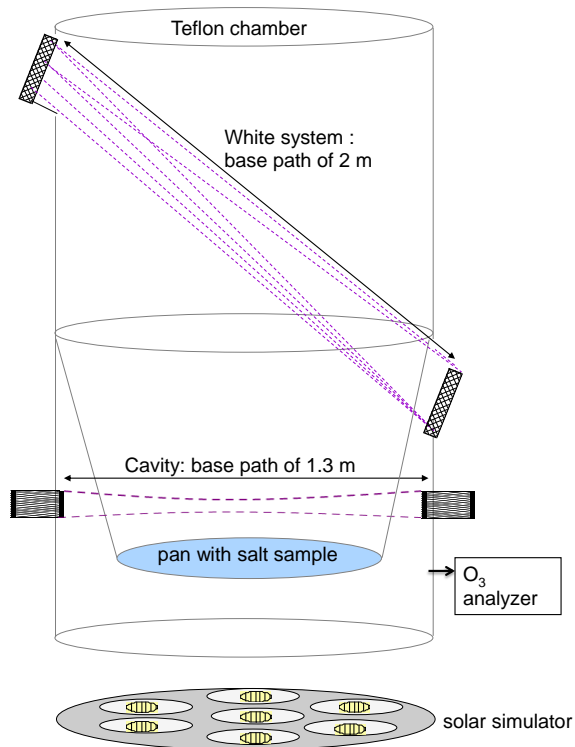


Fig. 9. Sketch of the multi-reflection cells used for DOAS in the teflon chamber. A White system with a base path of 2 m was installed on a diagonal frame. The mirrors and prisms of the White system were mounted inside the chamber with additional teflon bags. A maximum total light path of 320 m was achieved. The transfer optics adapts the opening aperture of the White system to the fiber and spectrograph. The CE-DOAS is mounted on a different frame, with a 1.3 m base path, resulting in an maximal light path of 816 m within this measurements (depending on the mirror reflectivity, here mirror set M_2 was used). The mirrors of the BrO-cavity constantly purged with clean air.

Title Page

Abstract

Introduction

Conclusions

References

Tables

Figures

⏪

⏩

◀

▶

Back

Close

Full Screen / Esc

Printer-friendly Version

Interactive Discussion



BrO CE-DOAS

D. J. Hoch et al.

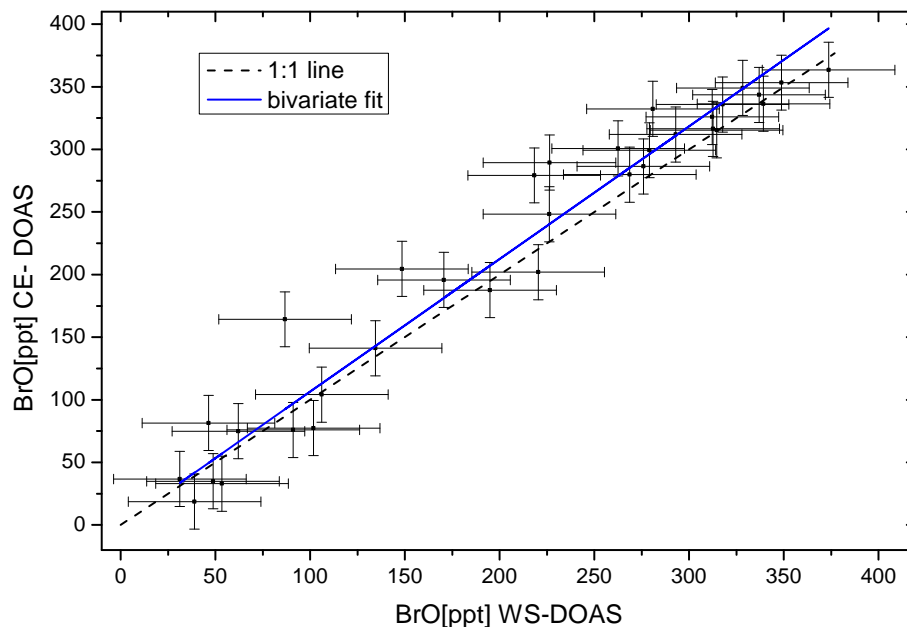


Fig. 10. Intercomparison for BrO detected by the White system and CE-DOAS simultaneously during a smog chamber experiment above a simulated salt pan, without injection of aerosols. The slope of the BrO mixing ratios measured by each instrument is 1.06 ± 0.07 using a bivariate weighted fit. The correlation coefficient is $r^2 = 0.95$.

[Title Page](#)[Abstract](#)[Introduction](#)[Conclusions](#)[References](#)[Tables](#)[Figures](#)[◀](#)[▶](#)[◀](#)[▶](#)[Back](#)[Close](#)[Full Screen / Esc](#)[Printer-friendly Version](#)[Interactive Discussion](#)

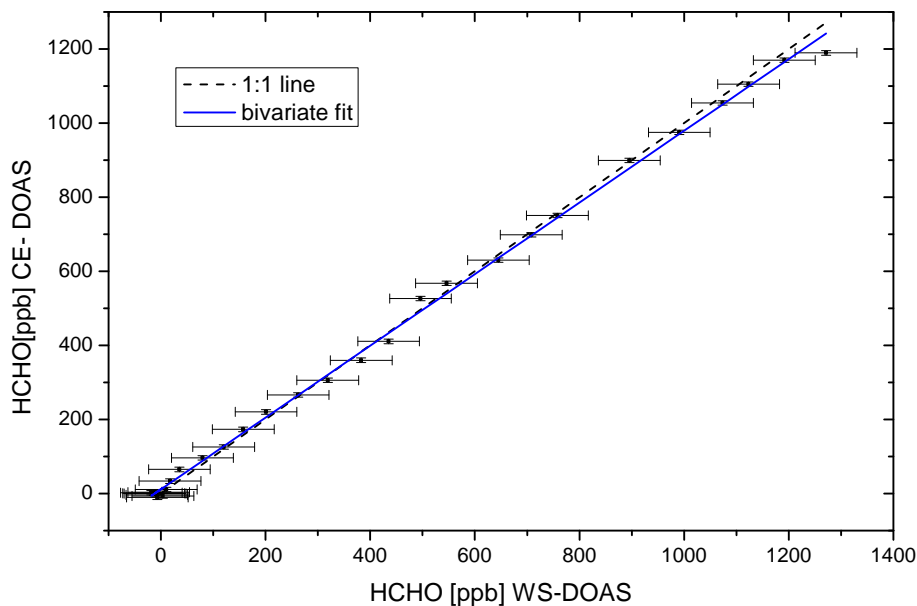


Fig. 11. Intercomparison for formaldehyde detected by the White system and CE-DOAS simultaneously during a smog chamber experiment above a simulated salt pan, without injection of aerosols. The slope of the HCHO mixing ratios measured by each instrument is 0.97 ± 0.03 using a bivariate weighted fit. The correlation coefficient is $r^2 = 0.998$.

[Title Page](#)[Abstract](#)[Introduction](#)[Conclusions](#)[References](#)[Tables](#)[Figures](#)[◀](#)[▶](#)[◀](#)[▶](#)[Back](#)[Close](#)[Full Screen / Esc](#)[Printer-friendly Version](#)[Interactive Discussion](#)

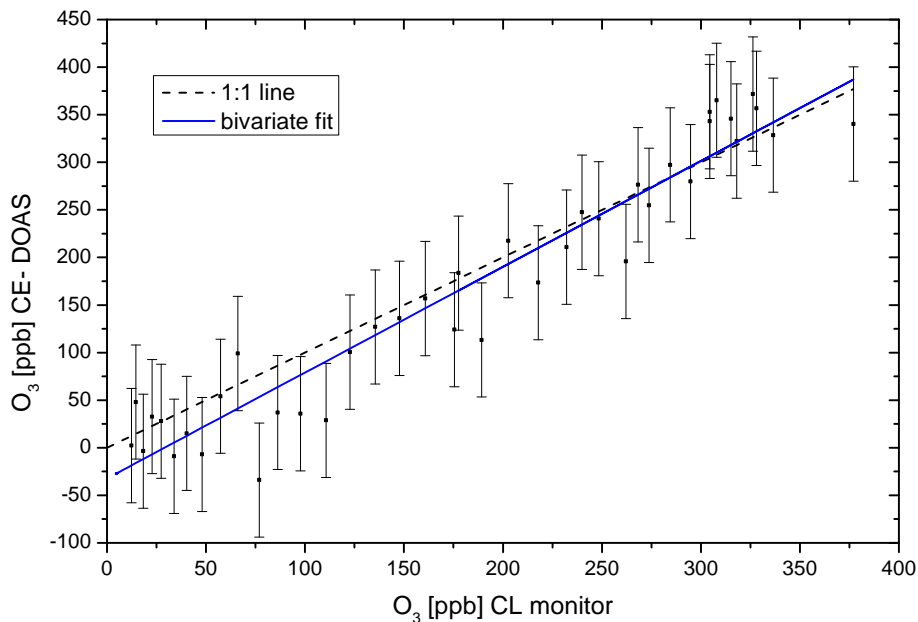


Fig. 12. Intercomparison for O₃ detected by the ozone monitor and CE-DOAS simultaneously during a smog chamber experiment above a simulated salt pan, without injection of aerosols. The slope of the O₃ mixing ratios measured by each instrument is 1.11 ± 0.08 using a bivariate weighted fit. The correlation coefficient is $r^2 = 0.92$.

[Title Page](#)[Abstract](#)[Introduction](#)[Conclusions](#)[References](#)[Tables](#)[Figures](#)[◀](#)[▶](#)[◀](#)[▶](#)[Back](#)[Close](#)[Full Screen / Esc](#)[Printer-friendly Version](#)[Interactive Discussion](#)

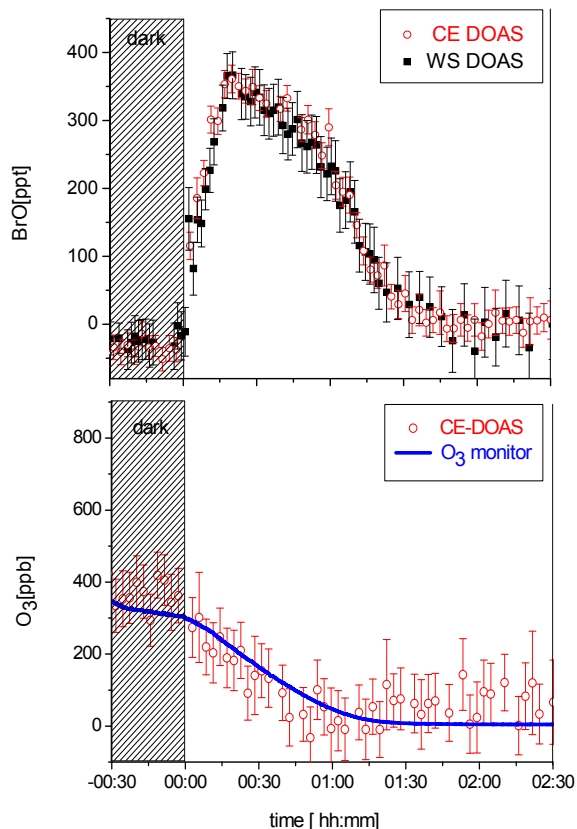


Fig. 13. Inter comparison of a time series of BrO (top panel) detected by the WS (black squares) and CE-DOAS (red open cycles) and O₃ (bottom panel) detected by the CE-DOAS (red open cycles) and O₃ monitor (blue line) simultaneously during a smog chamber experiment above a simulated salt pan. BrO is formed under irradiation (360 ppt within 17 min) and decreases to less than 30 ppt after 2 h. A corresponding total depletion of 320 ppb O₃ after 150 min is observed during the irradiation by the solar simulator.